(Fig. 4*B*, genotype and treatment main effects, and interaction effect in IIA, P = NS by two-way ANOVA) was small (~1%) and similar between control and CB-treated mice in both WT (1.0 ± 0.4 *vs.* 0.5 ± 0.2%, P = NS by Tukey's test, n = 6) and Epac1KO (0.6 ± 0.3 *vs.* 0.7 ± 0.3%, P = NS by Tukey's test, n = 6). These results indicate that the masseter muscle was primarily composed of type IID/X fibre and type IIB fibre, in agreements with the SDS-PAGE analysis (Fig. 3). CB treatment significantly decreased the proportion of type IID/X fibre (Fig. 4*B*, significant treatment main effect in IID/X, $P < 0.01$ by two-way ANOVA) in both WT (from 67 ± 3.8 to 49 ± 2.4%, $P < 0.01$ by Tukey's test, n = 6) and Epac1KO (from 64 ± 2.4 to 50 ± 3.6%, $P < 0.05$ by Tukey's test, n = 6), but it significantly increased the proportion of type IIB fibre (Fig. 4*B*, significant treatment main effect in IIB,

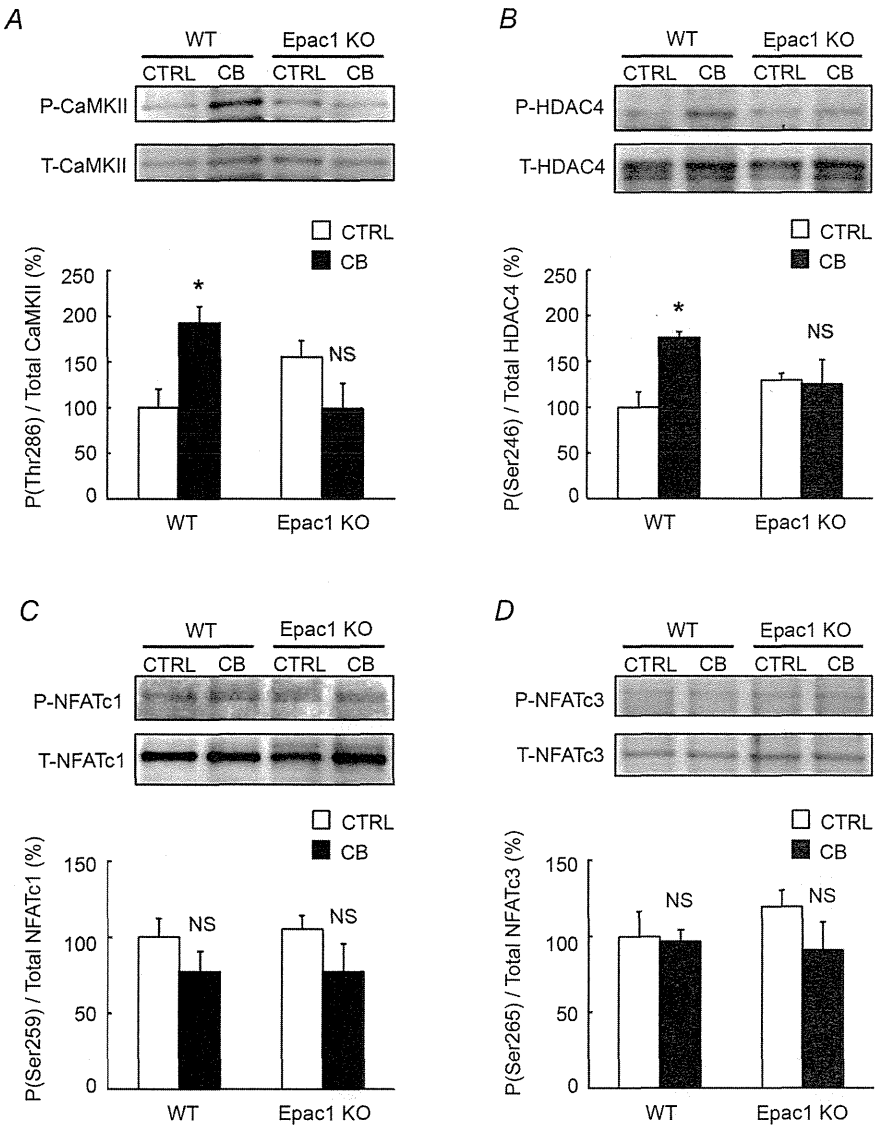

Figure 6. Activities of CaMKII/HDAC4 or calcineurin/NFAT signaling in WT and Epac1KO in response to chronic CB treatment
A-B, phosphorylated and total CaMKII (*A*) and HDAC4 (*B*) in masseter muscle of WT and Epac1KO were examined after chronic CB treatment (2 mg kg^{-1} day^{-1} I.P.) for 3 weeks. Phosphorylation of both CaMKII and HDAC4 was significantly increased in WT (*$P < 0.05$ by Tukey's *post hoc* test, n = 5–6), but the increases were suppressed in Epac1KO (P = NS, n = 5–6 by Tukey's *post hoc* test). *C-D*, phosphorylated and total NFATc1 (*C*) and NFATc3 (*D*) in masseter muscle of WT and Epac1KO were examined after CB treatment for 3 weeks. Phosphorylation of NFATc1 and NFATc3 tended to be decreased, though not significantly, in both WT and Epac1KO (P = NS by Tukey's *post hoc* test, n = 6)

$P < 0.01$ by two-way ANOVA) in both WT (from 32 ± 3.9 to 50 ± 2.4%, $P < 0.01$ by Tukey's test, n = 6) and Epac1KO (from 36 ± 2.2 to 49 ± 3.7%, $P < 0.05$ by Tukey's test, $n = 6$). The results of NADH-TR staining showed that the oxidative capacity of muscle fibres followed the pattern IIA (dark) > IID/X > IIB (light), as shown previously (Fig. 4*A*, lower) (Hamalainen and Pette, 1993; Sartorius *et al.* 1998). These data indicated that Epac1 did not influence the slow-to-fast MHC isoform transition in the masseter muscle in response to CB treatment, in accordance with the SDS-PAGE findings.

CB-mediated Akt pathway activation was attenuated in Epac1KO

Activation of β_2-AR was shown to activate Akt via the Giα-G$\beta\gamma$-PI3K pathway in cardiac myocytes (Zhu *et al.* 2001). Recently, we reported that Akt/mTOR is involved in both development of hypertrophy and fast-to-slow MHC isoform transition in masseter muscle in response to mechanical overload stress (Umeki *et al.* 2013). However, the role of Epac1 in β_2-AR-mediated masseter muscle hypertrophy and activation of the Akt/mTOR pathway remains poorly understood.

Thus, we first examined the Akt phosphorylation on serine 473 (Fig. 5*A*, significant interaction effect, $P < 0.05$ by two-way ANOVA) and confirmed that it was significantly increased in WT, but not in Epac1KO (WT *vs.* Epac1KO: from 100 ± 9.4 to 161 ± 19%, $P < 0.05$ by Tukey's test, $n = 5$ *vs.* from 96 ± 21 to 90 ± 7.7%, $P =$ NS by Tukey's test, $n = 5$–6).

We also examined the phosphorylation of Akt downstream target, glycogen synthase kinase-3β (GSK-3β) (Fig. 5*B*, significant interaction effect, $P < 0.01$ by two-way ANOVA), because GSK-3β activity is negatively regulated by Akt activity (Hardt and Sadoshima, 2002; Okumura *et al.* 2007). The phosphorylation level of GSK-3β at serine 9 was significantly increased in masseter muscle of WT (from 100 ± 23 to 206 ± 38%, $P < 0.05$ by Tukey's test, $n = 5$–6), but this increase was suppressed in Epac1KO (from 127 ± 10 to 83 ± 18%, $P =$ NS by Tukey's test, $n = 5$–6).

We next examined activation of the Akt/mTOR pathway in terms of phosphorylation of S6K1 on threonine 389 (Fig. 5*C*, significant interaction effect, $P < 0.05$ by two-way ANOVA) and eukaryotic initiation factor 4E-binding protein 1 (4E-BP1) on threonine 37/46 (Fig. 5*D*, significant interaction effect, $P < 0.05$ by two-way ANOVA). We found that these phosphorylations were significantly increased by CB treatment in masseter muscle of WT (S6K1: from 100 ± 16 to 159 ± 14%; 4E-BP1: from 100 ± 18 to 184 ± 18, $P < 0.05$ by Tukey's test, $n = 5$–6), but these increases were suppressed in Epac1KO (S6K1: from 124 ± 16 to 107 ± 12%; 4E-BP1: from 121 ± 19 to 138 ± 19%, $P =$ NS by Tukey's test, $n = 5$). These data indicated that CB-mediated activation of Epac1/Akt/mTOR signalling might play an important role in the development of masseter muscle hypertrophy.

ERK pathway was attenuated in Epac1KO

We also examined the phosphorylation of p44/42 mitogen-activated protein kinase (also known as ERK1/2) on threonine 202/tyrosine 204, because β_2-AR activation has been shown to phosphorylate ERK1/2 via the Giα-G$\beta\gamma$ pathway in skeletal muscle (Zhu *et al.* 2001) (Fig. 5*E*, significant interaction effect, $P < 0.05$ by two-way ANOVA). Also, ERK1/2 phosphorylation was reported to be necessary for regulating the mass of skeletal muscle by us and another group (Penna *et al.* 2010*a*; Umeki *et al.* 2013).

Phosphorylation of ERK1/2 in masseter muscle was similar between the control and CB-treated groups in WT (Control *vs.* CB: 100 ± 12 *vs.* 79 ± 8%, $P =$ NS by Tukey's test, $n = 5$), but CB induced a significant increase of phosphorylation by approximately 2-fold in Epac1KO (Control *vs.* CB: 126 ± 21 *vs.* 236 ± 42%, $P < 0.05$ by Tukey's test, $n = 5$) (Fig. 5*E*). These data indicate that Epac1 decreased the CB-mediated activation of ERK1/2 signalling in masseter muscle.

CaMKII/HDAC4 pathway was attenuated in Epac1KO

Phosphorylation of histone deacetylase 4 (HDAC4) on serine 265/266 mediated by PKA leads to induction of skeletal muscle atrophy, whereas phosphorylation on serine 246 mediated by Epac-activated calmodulin kinase II (CaMKII) leads to induction of skeletal muscle hypertrophy (Liu and Schneider, 2013).

We thus examined the phosphorylation of CaMKII on threonine 286 (Fig. 6*A*, significant interaction effect, $P < 0.01$ by two-way ANOVA) and HDAC4 on serine 246 (Fig. 6*B*, significant interaction effect, $P < 0.05$ by two-way ANOVA) in CB-treated masseter muscle of WT and Epac1KO. These phosphorylations were significantly increased in WT (CaMKII: from 100 ± 20 to 192 ± 18%, $n = 6$, $P < 0.05$ by Tukey's test; HDAC4: from 100 ± 16 to 176 ± 6.6%, $n = 5$–6, $P < 0.05$ by Tukey's test), but the increases were suppressed in Epac1KO (CaMKII: from 156 ± 18 to 99 ± 28%, $P =$ NS by Tukey's test, $n = 6$; HDAC4: from 130 ± 7.2 to 125 ± 27%, $P =$ NS by Tukey's test, $n = 5$). These data suggest that Epac1 plays an important role in development of masseter muscle hypertrophy through the regulation of CaMKII/HDAC4 activity, in addition to activation of Akt/mTOR signalling.

Calcineurin-NFAT signalling was not altered in Epac1KO

Calcineurin is a calcium/calmodulin-regulated protein phosphatase that acts on the transcription factors of the nuclear factor of activated T cells (NFAT) family, causing them to be translocated to the nucleus, where they induce transcriptional activation. We have previously demonstrated that calcineurin-NFAT signalling has a role in preservation of masseter muscle mass (Arai *et al.* 2005). Therefore, we examined the role of Epac1 in calcineurin-NFAT signalling activation in response to chronic CB treatment. We found that phosphorylation of NFATc1 on serine 259 (Fig. 6*C*, genotype and treatment main effects, and interaction effects, P = NS by two-way ANOVA) and NFATc3 on serine 265 (Fig. 6*D*, genotype and treatment main effects, and interaction effects, P = NS by two-way ANOVA) tended to be decreased, though not significantly, in both WT and Epac1KO (NFATc1: WT: from 100 ± 12 to 77 ± 13%, Epac1KO: from 105 ± 9.1 to 77 ± 18%. NFATc3: WT: from 100 ± 16 to 97 ± 7.9%, Epac1KO: from 119 ± 11 to 91 ± 19%, P = NS by Tukey's test, $n = 6$) (Lunde *et al.* 2011). These data are consistent with the idea that Epac1 did not influence the activation of calcineurin-NFAT signalling in masseter muscle before or after CB treatment.

Discussion

Most skeletal muscle growth-promoting agonists, such as CB and salbutamol, are highly selective for β_2-AR, and their action is thought to occur through Gsα-AC-cAMP-PKA signalling via β_2-AR with slow-to-fast MHC isoform transition (Li *et al.* 2012; Ohnuki *et al.* 2013*a*). Recently, it was reported that β_2-AR couples not only to Gsα, but also to Giα in skeletal muscle, leading to stimulation of G$\beta\gamma$-mediated Akt signalling as well as ERK1/2 signalling (Fig. 7) (Zhu *et al.* 2001; Gosmanov *et al.* 2002; Shi *et al.* 2007). We have recently demonstrated that both CB, a lipophilic β_2-AR agonist, and salbutamol, a hydrophilic β_2-AR agonist, similarly induce masseter muscle hypertrophy with slow-to-fast MHC isoform transition, indicating that hypertrophy might be mediated through direct muscle β_2-AR stimulation, not through CNS β_2-AR stimulation (Ohnuki *et al.* 2013*a*). However, the relationship between cAMP signalling and Akt or ERK1/2 signalling in skeletal muscle hypertrophy as well as MHC isoform transition remains poorly understood.

We hypothesized that Epac1, which was recently identified as a PKA-independent cAMP sensor and a major skeletal muscle isoform, might play an important role in masseter muscle hypertrophy and MHC isoform transition by linking cAMP signalling and Akt signalling or ERK signalling, and we aimed to test this hypothesis using Epac1-null mice (Okumura *et al.* 2014).

We first found that development of CB-mediated masseter muscle hypertrophy was suppressed in Epac1KO without any change of the slow-to-fast MHC isoform transition. Importantly, phosphorylation of Akt on serine 473 and its downstream molecules S6K1 on serine 389 and 4E-BP1 on threonine 37/46, and, in parallel, GSK-3β on serine 9 by CB treatment were all inhibited in Epac1KO without affecting the MHC isoform transition towards faster isoforms. These data indicated that CB-mediated masseter muscle hypertrophy might develop as a result of activation of cAMP/Epac1/Akt signalling, rather than cAMP/PKA signalling, because the cAMP/PKA signalling

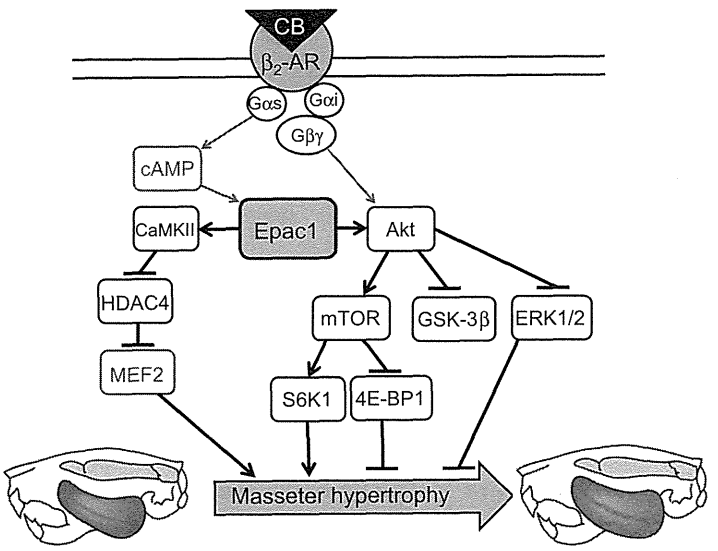

Figure 7. Schematic summary of the proposed role of Epac1 in masseter muscle hypertrophy
This scheme illustrates the proposed relationship between Epac1 and CB-mediated masseter muscle hypertrophy, mediated by activation of both Akt and CaMKII/HDAC4 signalings. Solid black lines represent findings in this study and solid grey lines represent findings reported previously (Kawasaki *et al.*, 1998, de Rooij *et al.*, 1998, Zhu *et al.*, 2001, Liu *et al.*, 2013).

in masseter muscle was intact in both WT and Epac1KO (Fig. 1*B*), as demonstrated previously in heart (Okumura *et al.* 2014). Conversely, Epac1 did not affect the MHC isoform transition toward faster isoforms induced by CB treatment in masseter muscle.

We recently demonstrated that phosphorylation of ERK1/2 on threonine 202/tyrosine 204 was reduced more in hypertrophied masseter muscle exposed to mechanical overload and the effect was attenuated by rapamycin, a selective mTOR inhibitor (Umeki *et al.* 2013). Our current data showed that ERK1/2 phosphorylation in masseter muscle was not different between WT and Epac1KO at baseline. However, it was significantly increased by approximately two-fold in masseter muscle of Epac1KO in response to CB treatment, though it remained unchanged in the hypertrophied masseter muscle of WT. Importantly, ERK activation was recently reported to be a critical contributor to muscle atrophy (Penna *et al.* 2010*a*). We thus anticipated that CB-mediated ERK1/2 phosphorylation in Epac1KO might be induced through the opposing effect of PI3-Akt signalling on ERK1/2 signalling, and up-regulation of ERK activity might be associated with the less effective CB-mediated hypertrophy in Epac1KO (Rommel *et al.* 1999; Penna *et al.* 2010*b*).

HDAC4 moves between cytoplasm and nuclei in cells prepared from flexor digitorum brevis muscle of CD-1 mice (Liu and Schneider, 2013). HDAC4 phosphorylation at serine 265/266 mediated by PKA induces nuclear influx, leading to inhibition of myocyte enhancer factor 2 (MEF2) activity, while phosphorylation at serine 246 mediated by CaMKII induces nuclear efflux, leading to activation of MEF2, which has a role in muscle hypertrophy (Fig. 7) (Potthoff *et al.* 2007; Cardinale *et al.* 2010). Importantly, Epac mediates the CaMKII-mediated HDAC4 phosphorylation on serine 246 (Liu and Schneider, 2013). We thus examined the phosphorylation of CaMKII on threonine 286 and HDAC4 on serine 246 in masseter muscle and found that these phosphorylations were significantly increased by CB treatment in masseter muscle of WT, but not in Epac1KO.

Taken together, the present finding indicate a causal relationship between Epac1 and CB-mediated masseter muscle hypertrophy and further suggest that this relationship might be mediated by the activation of both Akt signalling and CaMKII/HDAC4 signalling. As markers of the activation of Akt signalling, we examined the phosphorylation status of Akt itself and its downstream targets such as S6K1, 4E-BP1, and GSK-3β. Also, as markers of the activation of CaMKII/HDAC signalling, we examined the phosphorylation status of CaMKII and HDAC4. Phosphorylation of these markers was significantly increased in the masseter muscle of WT after CB infusion, but these increases were suppressed in Epac1KO.

Further studies will be required to determine whether activations of these signalling pathways were induced via stimulation of β_2-AR expressed in myofibres or vessel because direct myofibre β_2-AR stimulation was reported to increase protein synthesis and to decrease protein degradation, resulting in a net increase in myofibrillar protein content through activation of the Akt pathway or CaMKII/HDAC4 pathway (Choo *et al.* 1992; Joassard *et al.* 2013a; Joassard *et al.* 2013b; Liu and Schneider, 2013). Also, vascular β_2-AR stimulation in the masseter muscle was reported to evoke vasodilatation in the skeletal muscle and to induce endothelial nitric oxide synthase expression through the activation of the Akt and/or HDAC pathway (Rossig *et al.* 2002; Lee, 2002 Osuka *et al.* 2009; Ishii *et al.* 2010; Banquet *et al.* 2011; Bharti *et al.* 2012). Importantly, myocardial blood flow is pivotal for the development and maintenance of hypertrophied myocardium (Sano *et al.* 2007). In order to clarify the mechanisms involved at the molecular level, in vitro experiments using cultured skeletal muscle fibres and/or endothelial cells isolated from WT and Epac1KO might be a fruitful approach Liu and (Schneider, 2013; Liu *et al.* 2014), and we are planning studies along this line.

In view of the current finding that disruption of Epac1 inhibited the development of CB-mediated masseter muscle hypertrophy, we consider that pharmacological activation of Epac1 might be an alternative approach for the treatment of masticatory dysfunction due to masseter muscle wasting and weakness.

References

Altarejos JY & Montminy M (2011). CREB and the CRTC co-activators: sensors for hormonal and metabolic signals. *Nat Rev Cell Biol* **12**, 141–151.

Arai C, Ohnuki Y, Umeki D & Saeki Y (2005). Effects of bite-opening and cyclosporin A on the mRNA levels of myosin heavy chain and the muscle mass in rat masseter. *Jpn J Physiol* **55**, 173–179.

Bai Y, Tsunematsu T, Jiao Q, Ohnuki Y, Mototani Y, Shiozawa K, Jin M, Cai W, Jin HL, Fujita T, Ichikawa Y, Suita K, Kurotani R, Yokoyama U, Sato M, Iwatsubo K, Ishikawa Y & Okumura S (2012). Pharmacological stimulation of type 5 adenylyl cyclase stabilizes heart rate under both microgravity and hypergravity induced by parabolic flight. *J Pharmacol Sci* **119**, 381–389.

Banquet S, Delannoy E, Agouni A, Dessy C, Lacomme S, Hubert F, Richard V, Muller B & Leblais V (2011). Role of $G_{i/o}$-Src kinase-PI3K/Akt pathway and caveolin-1 in β_2-adrenoceptor coupling to endothelial NO synthase in mouse pulmonary artery. *Cell Signal* **23**, 1136–1143.

Bharti S, Singh R, Chauhan SS, Hussain T, Al-Attas OS & Arya DS (2012). Phosphorylation of Akt/GSK-3β/eNOS amplifies 5-HT_{2B} receptor blockade mediated anti-hypertrophic effect in rats. *FEBS Lett* **586**, 180–185.

Brennesvik EO, Ktori C, Ruzzin J, Jebens E, Shepherd PR & Jensen J (2005). Adrenaline potentiates insulin-stimulated PKB activation via cAMP and Epac: implications for cross talk between insulin and adrenaline. *Cell Signal* **17**, 1551–1559.

Bruusgaard JC, Egner IM, Larsen TK, Dupre-Aucouturier S, Desplanches D & Gundersen K (2012). No change in myonuclear number during muscle unloading and reloading. *J Appl Physiol (1985)* **113**, 290–296.

Cardinale JP, Sriramula S, Pariaut R, Guggilam A, Mariappan N, Elks CM & Francis J (2010). HDAC inhibition attenuates inflammatory, hypertrophic, and hypertensive responses in spontaneously hypertensive rats. *Hypertension* **56**, 437–444.

Choo JJ, Horan MA, Little RA & Rothwell NJ (1992). Anabolic effects of clenbuterol on skeletal muscle are mediated by β_2-adrenoceptor activation. *Am J Physiol Endocrinol Metab* **263**, E50–E56.

de Rooij J, Zwartkruis FJ, Verheijen MH, Cool RH, Nijman SM, Wittinghofer A & Bos JL (1998). Epac is a Rap1 guanine-nucleotide-exchange factor directly activated by cyclic AMP. *Nature* **396**, 474–477.

Farber E, Sternberg WH & Dunlap CE (1954). Tetrazolium stains for diphosphopyridine nucleotide (DPN) diaphorase and triphosphopyridine nucleotide (TPN) diaphorase in animal tissue. *Proc Soc Exp Biol Med* **86**, 534–537.

Goodman CA, Frey JW, Mabrey DM, Jacobs BL, Lincoln HC, You JS & Hornberger TA (2011). The role of skeletal muscle mTOR in the regulation of mechanical load-induced growth. *J Physiol* **589**, 5485–5501.

Gosmanov AR, Wong JA & Thomason DB (2002). Duality of G protein-coupled mechanisms for β-adrenergic activation of NKCC activity in skeletal muscle. *Am J Physiol Cell Physiol* **283**, C1025–C1032.

Hämäläinen N & Pette D (1993). The histochemical profiles of fast fiber types IIB, IID, and IIA in skeletal muscles of mouse, rat, and rabbit. *J Histochem Cytochem* **41**, 733–743.

Hardt SE & Sadoshima J (2002). Glycogen synthase kinase-3β: a novel regulator of cardiac hypertrophy and development. *Circ Res* **90**, 1055–1063.

Ishii H, Niioka T & Izumi H (2010). Vagal visceral inputs to the nucleus of the solitary tract: involvement in a parasympathetic reflex vasodilator pathway in the rat masseter muscle. *Brain Res* **1312**, 41–53.

Joassard OR, Amirouche A, Gallot YS, Desgeorges MM, Castells J, Durieux AC, Berthon P & Freyssenet DG (2013*a*). Regulation of Akt-mTOR, ubiquitin-proteasome and autophagy-lysosome pathways in response to formoterol administration in rat skeletal muscle. *Int J Biochem Cell Biol* **45**, 2444–2455.

Joassard OR, Durieux AC & Freyssenet DG (2013*b*). β_2-Adrenergic agonists and the treatment of skeletal muscle wasting disorders. *Int J Biochem Cell Biol* **45**, 2309–2321.

Kawasaki H, Springett GM, Mochizuki N, Toki S, Nakaya M, Matsuda M, Housman DE & Graybiel AM (1998). A family of cAMP-binding proteins that directly activate Rap1. *Science* **282**, 2275–2279.

Kiliaridis S, Engström C & Thilander B (1988). Histochemical analysis of masticatory muscle in the growing rat after prolonged alteration in the consistency of the diet. *Arch Oral Biol* **33**, 187–193.

Kim YS, Sainz RD, Molenaar P & Summers RJ (1991). Characterization of β_1- and β_2-adrenoceptors in rat skeletal muscles. *Biochem Pharmacol* **42**, 1783–1789.

Lee TJ(2002). Sympathetic modulation of nitrergic neurogenic vasodilation in cerebral arteries. *Jpn J Pharmacol* **88**, 26–31.

Li Y, He J, Sui S, Hu X, Zhao Y & Li N (2012). Clenbuterol upregulates histone demethylase JHDM2a via the β_2-adrenoceptor/cAMP/PKA/p-CREB signaling pathway. *Cell Signal* **24**, 2297–2306.

Liu QS, Wang HF, Sun AK, Huo XP, Liu JL, Ma SH, Peng N & Hu J (2014). A comparative study on inhibition of total astragalus saponins and astragaloside IV on TNFR1-mediated signaling pathways in arterial endothelial cells. *PloS One* **9**, e101504.

Liu Y & Schneider MF (2013). Opposing HDAC4 nuclear fluxes due to phosphorylation by β-adrenergic activated protein kinase A or by activity or Epac activated CaMKII in skeletal muscle fibres. *J Physiol* **591**, 3605–3623.

Lunde IG, Kvaloy H, Austbo B, Christensen G & Carlson CR (2011). Angiotensin II and norepinephrine activate specific calcineurin-dependent NFAT transcription factor isoforms in cardiomyocytes. *J Appl Physiol (1985)* **111**, 1278–1289.

Lynch GS & Ryall JG (2008). Role of β-adrenoceptor signaling in skeletal muscle: implications for muscle wasting and disease. *Physiol Rev* **88**, 729–767.

Machholz E, Mulder G, Ruiz C, Corning BF & Pritchett-Corning KR (2012). Manual restraint and common compound administration routes in mice and rats. *J Vis Exp* **67**, e2771.

Ohnuki Y, Kawai N, Tanaka E, Langenbach GE, Tanne K & Saeki Y (2009). Effects of increased occlusal vertical dimension on daily activity and myosin heavy chain composition in rat jaw muscle. *Arch Oral Biol* **54**, 783–789.

Ohnuki Y & Saeki Y (2008). Jaw-opening muscle contracts more economically than jaw-closing muscle in rat. *Arch Oral Biol* **53**, 193–198.

Ohnuki Y, Saeki Y, Yamane A, Kawasaki K & Yanagisawa K (1999). Adaptation of guinea-pig superficial masseter muscle to an increase in occlusal vertical dimension. *Arch Oral Biol* **44**, 329–335.

Ohnuki Y, Umeki D, Cai W, Kawai N, Mototani Y, Shiozawa K, Jin HL, Fujita T, Tanaka E, Saeki Y & Okumura S (2013*a*). Role of masseter muscle β_2-adrenergic signaling in regulation of muscle activity, myosin heavy chain transition, and hypertrophy. *J Pharmacol Sci* **123**, 36–46.

Ohnuki Y, Yamada T, Mototani Y, Umeki D, Shiozawa K, Fujita T, Saeki Y & Okumura S (2013*b*). Effects of protein kinase A on the phosphorylation status and transverse stiffness of cardiac myofibrils. *J Pharmacol Sci* **123**, 279–283.

Okumura S, Fujita T, Cai W, Jin M, Namekata I, Mototani Y, Jin H, Ohnuki Y, Tsuneoka Y, Kurotani R, Suita K, Kawakami Y, Hamaguchi S, Abe T, Kiyonari H, Tsunematsu T, Bai Y, Suzuki S, Hidaka Y, Umemura M, Ichikawa Y, Yokoyama U, Sato M, Ishikawa F, Izumi-Nakaseko H, Adachi-Akahane S, Tanaka H & Ishikawa Y (2014). *Epac1*-dependent phospholamban phosphorylation mediates the cardiac response to stresses. *J Clin Invest* **124**, 2785–2801.

Okumura S, Kawabe J, Yatani A, Takagi G, Lee MC, Hong C, Liu J, Takagi I, Sadoshima J, Vatner DE, Vatner SF & Ishikawa Y (2003*a*). Type 5 adenylyl cyclase disruption alters not only sympathetic but also parasympathetic and calcium-mediated cardiac regulation. *Circ Res* **93**, 364–371.

Okumura S, Suzuki S & Ishikawa Y (2009). New aspects for the treatment of cardiac diseases based on the diversity of functional controls on cardiac muscles: effects of targeted disruption of the type 5 adenylyl cyclase gene. *J Pharmacol Sci* **109**, 354–359.

Okumura S, Takagi G, Kawabe J, Yang G, Lee MC, Hong C, Liu J, Vatner DE, Sadoshima J, Vatner SF & Ishikawa Y (2003*b*). Disruption of type 5 adenylyl cyclase gene preserves cardiac function against pressure overload. *Proc Natl Acad Sci USA* **100**, 9986–9990.

Okumura S, Tsunematsu T, Bai Y, Jiao Q, Ono S, Suzuki S, Kurotani R, Sato M, Minamisawa S, Umemura S & Ishikawa Y (2008). Type 5 adenylyl cyclase plays a major role in stabilizing heart rate in response to microgravity induced by parabolic flight. *J Appl Physiol (1985)* **105**, 173–179.

Okumura S, Vatner DE, Kurotani R, Bai Y, Gao S, Yuan Z, Iwatsubo K, Ulucan C, Kawabe J, Ghosh K, Vatner SF & Ishikawa Y (2007). Disruption of type 5 adenylyl cyclase enhances desensitization of cyclic adenosine monophosphate signal and increases Akt signal with chronic catecholamine stress. *Circulation* **116**, 1776–1783.

Osuka K, Watanabe Y, Usuda N, Atsuzawa K, Yoshida J & Takayasu M (2009). Modification of endothelial nitric oxide synthase through AMPK after experimental subarachnoid hemorrhage. *J Neurotrauma* **26**, 1157–1165.

Pearen MA, Ryall JG, Lynch GS & Muscat GE (2009). Expression profiling of skeletal muscle following acute and chronic β_2-adrenergic stimulation: implications for hypertrophy, metabolism and circadian rhythm. *BMC Genomics* **10**, e448.

Penna F, Bonetto A, Muscaritoli M, Costamagna D, Minero VG, Bonelli G, Rossi Fanelli F, Baccino FM & Costelli P (2010*a*). Muscle atrophy in experimental cancer cachexia: is the IGF-1 signaling pathway involved? *Int J Cancer* **127**, 1706–1717.

Penna F, Costamagna D, Fanzani A, Bonelli G, Baccino FM & Costelli P (2010*b*). Muscle wasting and impaired myogenesis in tumor bearing mice are prevented by ERK inhibition. *PloS One* **5**, e13604.

Potthoff MJ, Wu H, Arnold MA, Shelton JM, Backs J, McAnally J, Richardson JA, Bassel-Duby R & Olson EN (2007). Histone deacetylase degradation and MEF2 activation promote the formation of slow-twitch myofibers. *J Clin Invest* **117**, 2459–2467.

Rommel C, Clarke BA, Zimmermann S, Nuñez L, Rossman R, Reid K, Moelling K, Yancopoulos GD & Glass DJ (1999). Differentiation stage-specific inhibition of the Raf-MEK-ERK pathway by Akt. *Science* **286**, 1738–1741.

Rossig L, Li H, Fisslthaler B, Urbich C, Fleming I, Forstermann U, Zeiher AM & Dimmeler S (2002). Inhibitors of histone deacetylation downregulate the expression of endothelial nitric oxide synthase and compromise endothelial cell function in vasorelaxation and angiogenesis. *Circ Res* **91**, 837–844.

Ryall JG, Gregorevic P, Plant DR, Sillence MN & Lynch GS (2002). β_2-Agonist fenoterol has greater effects on contractile function of rat skeletal muscles than clenbuterol. *Am J Physiol Regul Integr Comp Physiol* **283**, R1386–R1394.

Sano M, Minamino T, Toko H, Miyauchi H, Orimo M, Qin Y, Akazawa H, Tateno K, Kayama Y, Harada M, Shimizu I, Asahara T, Hamada H, Tomita S, Molkentin JD, Zou Y & Komuro I (2007). p53-induced inhibition of Hif-1 causes cardiac dysfunction during pressure overload. *Nature* **446**, 444–448.

Sartorius CA, Lu BD, Acakpo-Satchivi L, Jacobsen RP, Byrnes WC & Leinwand LA (1998). Myosin heavy chains IIa and IId are functionally distinct in the mouse. *J Cell Biol* **141**, 943–953.

Shi H, Zeng C, Ricome A, Hannon KM, Grant AL & Gerrard DE (2007). Extracellular signal-regulated kinase pathway is differentially involved in β-agonist-induced hypertrophy in slow and fast muscles. *Am J Physiol Cell Physiol* **292**, C1681–C1689.

Suzuki S, Yokoyama U, Abe T, Kiyonari H, Yamashita N, Kato Y, Kurotani R, Sato M, Okumura S & Ishikawa Y (2010). Differential roles of Epac in regulating cell death in neuronal and myocardial cells. *J Biol Chem* **285**, 24248–24259.

Turner PV, Brabb T, Pekow C & Vasbinder MA (2011*a*). Administration of substances to laboratory animals: routes of administration and factors to consider. *J Am Assoc Lab Anim Sci* **50**, 600–613.

Turner PV, Pekow C, Vasbinder MA & Brabb T (2011*b*). Administration of substances to laboratory animals: equipment considerations, vehicle selection, and solute preparation. *J Am Assoc Lab Anim Sci* **50**, 614–627.

Umeki D, Ohnuki Y, Mototani Y, Shiozawa K, Fujita T, Nakamura Y, Saeki Y & Okumura S (2013). Effects of chronic Akt/mTOR inhibition by rapamycin on mechanical overload-induced hypertrophy and myosin heavy chain transition in masseter muscle. *J Pharmacol Sci* **122**, 278–288.

Wong K, Boheler KR, Bishop J, Petrou M & Yacoub MH (1998). Clenbuterol induces cardiac hypertrophy with normal functional, morphological and molecular features. *Cardiovasc Res* **37**, 115–122.

Woo AY & Xiao RP (2012). β-Adrenergic receptor subtype signaling in heart: from bench to bedside. *Acta Pharmacol Sin* **33**, 335–341.

Yu H, He Y, Zhang X, Peng Z, Yang Y, Zhu R, Bai J, Tian Y, Li X, Chen W, Fang D & Wang R (2011). The rat IgGFcβBP and Muc2 C-terminal domains and TFF3 in two intestinal mucus layers bind together by covalent interaction. *PloS One* **6**, e20334.

Zhu WZ, Zheng M, Koch WJ, Lefkowitz RJ, Kobilka BK & Xiao RP (2001). Dual modulation of cell survival and cell death by β_2-adrenergic signaling in adult mouse cardiac myocytes. *Proc Natl Acad Sci USA* **98**, 1607–1612.

Additional information

Competing interests

None declared.

Author contributions

Y.O. and S.O. conceived and designed the research; Y.O., D.U., H.J. and W.C. performed the experiments; Y.O., Y.M., K. Shiozawa, K. Suita, Y.S., T.F., Y.I. and S.O. analysed the data; Y.O. and S.O. wrote the manuscript. All authors have read and approved the final version of the manuscript. All experiments were carried out at Tsurumi University and Yokohama City University.

Funding

This study was supported in part by the Japanese Ministry of Education, Culture, Sports, Science, and Technology (S.O., D.U., Y.M., T.F., Y.I.), a Grant-in-Aid for Scientific Research on Innovative Areas (22136009) (Y.I., S.O.), Takeda Science Foundation (S.O, Y.I.), Yokohama Foundation for Advancement of Medical Science (S.O., T.F.), Mitsubishi Pharma Research Foundation (S.O.), and Research for Promoting Technological Seeds A (discovery type) (S.O.), Yokohama Academic Foundation (Y.O., S.O.), 2010 Commercialization Promotion Program for Biotechnology-related Studies (S.O.), Grant for Research and Development Project II of Yokohama City University (S.O.), and Suzuken Memorial Foundation (S.O.).

Acknowledgements

We are grateful to Ms Yoko Shinoda (Tsurumi University, Yokohama, Japan) for assistance with graphics for publication.

Tsutsumi et al. Cardiovascular Diabetology 2014, 13:132
http://www.cardiab.com/content/13/1/132

CARDIO VASCULAR DIABETOLOGY

ORIGINAL INVESTIGATION Open Access

Exendin-4 ameliorates cardiac ischemia/reperfusion injury via caveolae and caveolins-3

Yasuo M Tsutsumi[1*†], Rie Tsutsumi[2†], Eisuke Hamaguchi[1], Yoko Sakai[1], Asuka Kasai[1], Yoshihiro Ishikawa[3], Utako Yokoyama[3] and Katsuya Tanaka[1]

Abstract

Background: Exendin-4, an exogenous glucagon-like peptide-1 receptor (GLP-1R) agonist, protects the heart from ischemia/reperfusion injury. However, the mechanisms for this protection are poorly understood. Caveolae, sarcolemmal invaginations, and caveolins, scaffolding proteins in caveolae, localize molecules involved in cardiac protection. We tested the hypothesis that caveolae and caveolins are essential for exendin-4 induced cardiac protection using *in vitro* and *in vivo* studies in control and caveolin-3 (Cav-3) knockout mice (Cav-3 KO).

Methods: Myocytes were treated with exendin-4 and then incubated with methyl-β-cyclodextrin (MβCD) to disrupt caveolae formation. This was then followed by simulated ischemia/reperfusion (SI/R). In addition, cardiac protection *in vivo* was assessed by measuring infarct size and cardiac troponin levels.

Results: Exendin-4 protected cardiac myocytes (CM) from SI/R [35.6 ± 12.6% vs. 64.4 ± 18.0% cell death, P = 0.034] and apoptosis but this protection was abolished by MβCD (71.8 ± 10.8% cell death, P = 0.004). Furthermore, Cav-3/GLP-1R co-localization was observed and membrane fractionation by sucrose density gradient centrifugation of CM treated with MβCD + exendin-4 revealed that buoyant (caveolae enriched) fractions decreased Cav-3 compared to CM treated with exendin-4 exclusively. Furthermore, exendin-4 induced a reduction in infarct size and cardiac troponin relative to control (infarct size: 25.1 ± 8.2% vs. 41.4 ± 4.1%, P < 0.001; troponin: 36.9 ± 14.2 vs. 101.1 ± 22.3 ng/ml, P < 0.001). However, exendin-4 induced cardiac protection was abolished in Cav-3 KO mice (infarct size: 43.0 ± 6.4%, P < 0.001; troponin: 96.8 ± 26.6 ng/ml, P = 0.001).

Conclusions: We conclude that caveolae and caveolin-3 are critical for exendin-4 induced protection of the heart from ischemia/reperfusion injury.

Keywords: Cardiac protection, Subcellular microdomain, Glucagon-like peptide-1 receptor, Incretin

Introduction

Glucagon-like peptide-1 (GLP-1) is an intestinal hormone secreted in a nutrient-dependent manner that stimulates insulin secretion and inhibits glucagon secretion and gastric emptying, resulting in reduced post-prandial hyperglycemia [1]. GLP-1 acts upon the GLP-1 receptor (GLP-1R), which belongs to the family of G-protein-coupled receptor (GPCRs) [2]. This receptor is abundantly expressed in the gastrointestinal tract, but has also been detected in the central nervous system, heart, vascular smooth muscle cells, endothelial cells, and macrophages [3,4]. Recently, GLP-1 has been shown to reduce an infarct size in both *in vitro* and *in vivo* animal models of cardiac ischemia/reperfusion injury [5-7] and exendin-4 (Ex-4), an exogenous GLP-1R agonist isolated form the Gila monster lizard [8], has reported to have very similar effects [4,9,10].

Caveolae are small flask-like invaginations of sarcolemmal membrane that are enriched in lipids. Caveolin-3 (Cav-3) is the principal protein component of caveolae and can interact with a number of signaling molecules including G protein, receptor tyrosine kinases, and GPCRs *via* caveolin-binding motif [11-13]. In our previous studies, we have shown that both caveolae and Cav-3 were essential in cardiac protection against ischemia/reperfusion in the animal model [14-17]. However, studies addressing the plasma-membrane localization

* Correspondence: tsutsumi@tokushima-u.ac.jp
†Equal contributors
[1]Department of Anesthesiology, University of Tokushima, 3-18-15 Kuramoto, Tokushima, Japan
Full list of author information is available at the end of the article

of GLP-1R are not fully known and the impact of caveolae and Cav-3 on GLP-1-induced cardiac protection has not been investigated. Therefore, we hypothesized that both caveolae and Cav-3 are a critical component of GLP-1-induced cardiac protection and that coordination of protective signaling is dependent on the co-localization of Cav-3 and GLP-1R.

Material and methods

All animals were treated in compliance with the Guidelines for Proper Conduct of Animal Experiment and Related Activities (Ministry of Education, Culture, Sports, Science and Technology of Japan) and the protocols, which was assigned to ARRIVE guidelines [18], approved by the Animal Care and Use Committee at the University of Tokushima. Male Wistar rats (12–14 weeks old, 250–300 g body weight) and male C57BL/6 mice (8–10 weeks old, 21–25 g body weight) were purchased from Japan SLC, and Cav-3 KO mice (8–10 weeks old, 21–25 g body weight) were created as reported previously [19]. The animals were kept on a 12 hour light–dark cycle in a temperature and humidity-controlled room, and had *ad lib* access to food and water.

Preparation of Cardiac Myocytes (CM)

CM were isolated from adult male Wistar rats as described [20,21]. In brief, hearts were retrograde perfused on a Langendorff apparatus and digested with collagenase (Worthington). Myocytes were plated in Medium 199 (4% fetal bovine serum and 1% penicillin/streptomycin) on laminin (2 μg/cm^2)-coated plates for 1 h. Plating media was changed to serum-free media (1% bovine serum albumin) to remove non-myocytes and CM were incubated for 24 h at 37°C in 5% CO_2.

Simulated ischemia/reperfusion (SI/R) in isolated cardiac myocytes

CM were plated on laminin-coated 12-well plates, and simulated ischemia was induced by replacing the air content with a 95% N_2 and 5% CO_2 gas mixture at 2 L/min in a chamber and by replacing the media to glucose-free media for 60 min. This was then followed by 60 min of "reperfusion" by replacing the media with normal maintenance media and by incubating the cells with 21% O_2 and 5% CO_2 [16]. CM were exposed to 0.3 nM or 3.0 nM Ex-4, a GLP-1R agonist, for 1 h prior to SI/R. Cell death was quantified by counting trypan blue-stained cells with results expressed as a percentage of total cells counted. Cells were counted (3 random fields per well) using ImageJ software to determine percent cell death. To determine the impact of caveolae on cardiac protection, methyl-β-cyclodextrin (MβCD) was used as described [16]. CM were incubated under maintenance media (control conditions) or in the presence of MβCD (1 mM) for 1 h before SI/R.

Depolarization of the mitochondrial membrane

To analyze mitochondrial membrane potential, we used the JC-1 dye (MitoPT JC-1, ImmunoChemistry Technologies, Bloomington, MN), which shifts the fluorescence emission from red (580 nm) to green (488 nm) as mitochondrial membrane is depolarized. After SI/R, as described above, myocytes were incubated with JC-1 for 20 min at 37°C, and cellular fluorescence was determined by a fluorescence microscope (Leica TCS NT, Heidelberg, Germany). Data are assessed by comparing the ratios of red/green.

Gene expression analyses

Total RNA was extracted from CM using RNeasy Plus Universal Mini Kits (QIAGEN, Valencia, CA). Total RNA (1 μg) was reverse-transcribed to cDNA in a final volume of 20 μL using the Primescript RT Reagent kit (Takara, Shiga, Japan). Real-time polymerase chain reaction (PCR) was performed in a final volume of 10 μL containing 50 ng of the cDNA template and primers using a StepOnePlus Real-Time PCR System (Life Technologies, Carlsbad, CA). To determine the effect on apoptosis gene expression, we measured the expression of the BH3-interacting domain death agonist (BID), Bcl-2-associated death promoter (BAD), Caspase-3, Caspase-8, and Caspase-9, and Bcl-2 associated X protein (BAX) genes. To determine the effect on anti-apoptosis gene expression, we measured the expression of the B-cell lymphoma 2 (BCL-2) and inhibitor of apoptosis 1 (IAP-1) genes.

Immunofluorescence

CM were fixed with paraformaldehyde, incubated with 100 mM glycine, permeabilized in 0.1% buffered Triton X-100, and blocked with 1% bovine serum albumin, phosphate-buffered saline, and 0.05% Tween. Samples were then incubated with primary antibody (GLP-1R and caveolins-3, Santa Cruz Biotechnology, Santa Cruz, CA) (1:100) in 1% bovine serum albumin, phosphate-buffered saline, and 0.05% Tween for 24 h. Excess antibody was removed, and samples were incubated with fluorescein Alexa-conjugated secondary antibodies (1:250) for 1 h. To remove excess secondary antibody, samples were washed with phosphate-buffered saline/0.1% Tween and samples were mounted in UltraCruz (Santa Cruz Bioctechnology) for microscopy imaging. Fluorescent images of cell sections excited at 488 and 560 nm were captured using a confocal laser scanning microscope (Leica TCS NT, Heidelberg, Germany) equipped with an argon-krypton laser source. Images were taken at 400 × magnification and were assessed quantitatively by Image-Pro Plus (Media Cybernetics, Silver Spring, MD).

Sucrose density fractionation

Whole left ventricles or myocytes were used for sucrose density membrane fractions as reported previously [22].

Briefly, approximately 1 ml of lysate was mixed with 1 ml of 80% sucrose in 25 mM MES and 150 mM NaCl (MES buffered saline, MBS, pH 6.5) to form 40% sucrose and loaded at the bottom of an ultracentrifuge tube. A discontinuous sucrose gradient was generated by layering 6 ml of 35% sucrose prepared in MBS followed by 4 ml of 5% sucrose in MBS. The gradient was centrifuged at 175,000 g using a P70AT2 rotor (Hitachi Koki Co.) for 3 h at 4°C. After centrifugation, samples were removed in 1 ml aliquots to yield 12 fractions. We defined fraction 4–6 as buoyant membrane fractions enriched in caveolae and proteins associated with caveolae. Fraction 9–12 were defined as nonbuoyant fractions.

Immunoprecipitation

Immunoprecipitation was performed using Protein A Sepharose CL-4B (GE Healthcare) as described previously [23]. Buoyant fraction samples were incubated with primary antibody (GLP-1R and caveolins-3, Santa Cruz Biotechnology) for 3 h at 4°C, immune-precipitated overnight with protein-agarose at 4°C, and then centrifuged for 5 min at 13,000 g. Protein-agarose pellets were washed 3 times. Wash buffer was removed and sample buffer was added, and then boiled for 5 min at 95°C for immunoblotting.

Immunoblot analysis

Proteins were separated by SDS-PAGE 10% polyacrylamide precast gels (Bio-Rad Laboratories) and transferred to a polyvinylidene diflouride membrane by electroelution. Membranes were blocked in PBS containing 2.0% nonfat dry milk and incubated with primary antibody overnight (GLP-1R and caveolins-3, Santa Cruz Biotechnology; GAPDH, Santa Cruz Biotechnology and Cell Signaling Technology) and at 4°C. Bound primary antibodies were visualized using secondary antibodies (Santa Cruz Biotechnology) conjugated with horseradish peroxidase from Santa Cruz Biotechnology and ECL reagent from GE Healthcare [24]. All displayed bands migrated at the appropriate size, as determined by comparison to molecular weight standards (Santa Cruz Biotechnology).

Ischemia/reperfusion protocol and experimental groups

C57BL/6 mice and Cav-3 knockout (Cav-3 KO) micewere anesthetized with pentobarbital sodium (80 mg/kg ip) and mechanically ventilated by using a pressure-controlled ventilator (TOPO Ventilator, Kent Scientific) as described before [25]. Core temperature was maintained with a heating pad and ECG leads were placed to record heart rate. The hemodynamic effects were measured through the right carotid artery cannulation with a 1.4 F Mikro-tip pressure transducer (Model SPR-671, Millar Instruments), which was connected to an amplifier (Model TC-510, Millar Instruments) for determination of heart rate, arterial blood pressure, and rate pressure product as previous before [26]. After thoracotomy, baseline was established, and mice were randomly assigned to experimental protocols. Lethal ischemia was produced by occluding the left coronary artery with a 7–0 silk suture on a taper BV-1 needle (Ethicon) for 30 min. After 30 min of occlusion, the ligature was released and the heart was reperfused for 2 h. After reperfusion, mice were heparinized, and the coronary artery was again occluded. The area at risk (AAR) was determined by staining with 1% Evans blue (Sigma). The heart was immediately excised and placed into 1% agarose and allowed to harden. Once hardened, the heart was cut into 1.0-mm slices (McIlwain tissue chopper; Brinkmann Instruments). Each slice of left ventricle (LV) was then counterstained with 2,3,5,-triphenyltetrazolium chloride (Sigma). After overnight storage in 10% formaldehyde, slices were weighed and visualized under a microscope (SZ61-TR, Olympus) equipped with a charge coupled device camera (DXM 1200 F, Nikon). The images were analyzed (Image-Pro Plus, Media Cybernetics), and AAR and infarct size (IS) was determined by planimetry as previously described [27,28]. Cardiac troponin I levels in the serum were measured using a High Sensitivity Mouse Cardiac Troponin-I ELISA Kit (Life Diagnostics).

Statistical analysis

Statistical analyses were performed by one-way and two-way ANOVA for repeated measures, followed by Bonferroni post-hoc test. All data are expressed as mean ± SD. Statistical significance was defined as $P < 0.05$.

Results

Experimental animals

The animals' health status was monitored throughout the experiments by a health surveillance program. A total of 98 animals were used in the experiments described here (35 animals for *in vitro* simulated ischemia/reperfusion, 23 for immunofluorescence and immunoblot analyses, and 40 for in vivo ischemia/reperfusion experiments). Five mice died shortly after ischemia/reperfusion because of fatal cardiac arrhythmia in the *in vivo* experiments (control, 1; Ex-4 administration, 2; Cav-3 KO control, 1; Cav-3 KO Ex-4 administration, 1).

Exendin-4 induces cardiac protection in CM

CM were administered with various concentration of Ex-4 and then SI/R (Figure 1A). Administration of 0.3 nM and 3.0 nM Ex-4 before SI/R decreased cell death when compared to SI/R alone (47.4 ± 9.9%, and 35.6 ± 12.6% and 64.4 ± 18.0% cell death, respectively, n = 5 per each groups; Figure 1B).

MβCD abolish exendin-4 induced cardiac protection

CM were incubated with 1% BSA with 0.1% penicillin/streptomycin (Control) or in control media along with

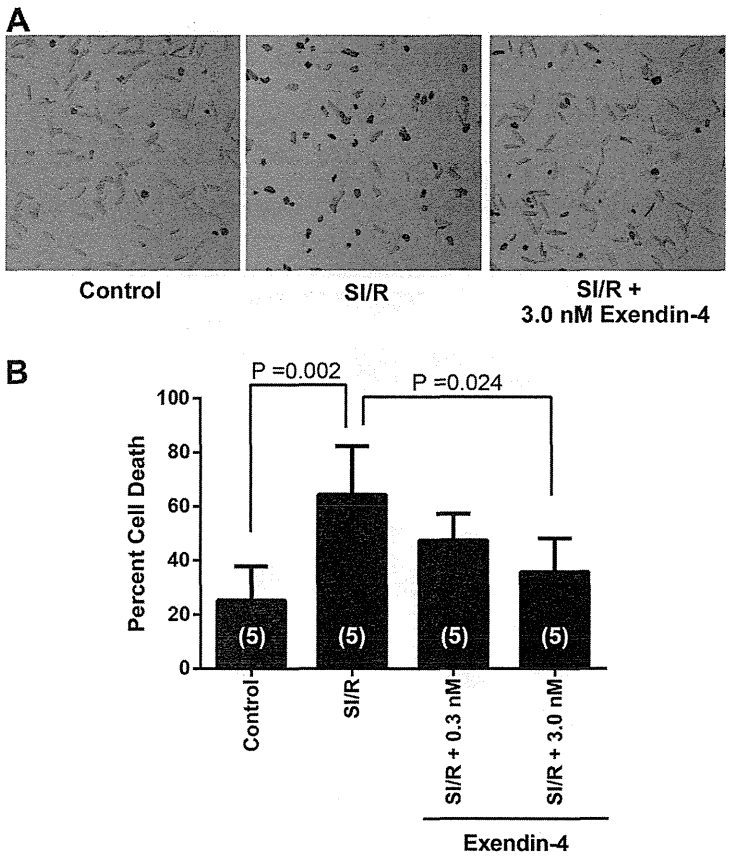

Figure 1 Effects of exendin-4 on simulated ischemia/reperfusion (SI/R) of cardiac myocytes. (A) Cardiac myocytes were rod-shaped and treated with various concentration of exendin-4 prior to exposure to SI/R. **(B)** Cell death was determined by trypan blue staining. Optimal protection was observed at 3.0 nM exendin-4. Group sizes are indicated on the individual bars in parentheses.

3.0 nM Ex-4, and/or then incubated with 1 mM MβCD (Figure 2A). In the present study, the protective effect of Ex-4 was abolished in CM with MβCD (35.6 ± 12.6% [n = 4] and 71.8 ± 10.8% [n = 5] cell death, respectively; P = 0.004). Additionally, we observed no significant increase in basal cell death with the various treatments (Figure 2B).

To test whether Ex-4 inhibited apoptosis by modifying the mitochondrial membrane potential during reperfusion injury, we measured a membrane potential-sensitive dye, 5,5',6,6'-tetrachloro-1,1',3,3'-tetraethylbenzamidazolocarbocyanin iodide (JC-1). As shown in Figure 2C, Ex-4 inhibited reduction of mitochondrial membrane potential that occurred in the re-oxygenated cells expressing SI/R suggesting inhibition of apoptosis. This was further confirmed as Ex-4 decreased pro-apoptic and increased anti-apoptotic gene expression (Figure 2D; n = 4 per each groups).

Co-localization between GLP-1R and Cav-3, and MβCD alter caveolins expression

Immunofluorescence microscopy showed that Cav-3 co-localizes with GLP-1R on the surface of the CM (Figure 3A). Co-immunoprecipitation experiments using cardiac lysates and antibodies to Cav-3 and GLP-1R provided further evidence for the interaction of these proteins (Figure 3B). Expression of Cav-3 in buoyant caveolar fractions (fractions 4–6) was significantly increased after administration of Ex-4 as compared with control mice, and Ex-4 induced migration of Cav-3 from non-buoyant to buoyant fraction was eliminated by MβCD (Figure 4).

Caveolin-3 is required for exendin-4 induced cardiac protection

To assess the role of Cav-3 in the protection from ischemia/reperfusion injury, we treated C57BL/6 wild-type mice or Cav-3 KO mice with Ex-4 administration, and then exposed the mice to ischemia/reperfusion (Figure 5A). We found no significant differences between groups in pre-occlusion heart rate, blood pressure, or rate pressure product with and without Ex-4 (Table 1). The ability of Ex-4 to protect from ischemia/reperfusion injury was abolished in Cav-3 KO mice compared to wild-type animals (43.0 ± 6.4% [n = 8] and 25.1 ± 8.2% [n = 7] IS/AAR, P < 0.001) even

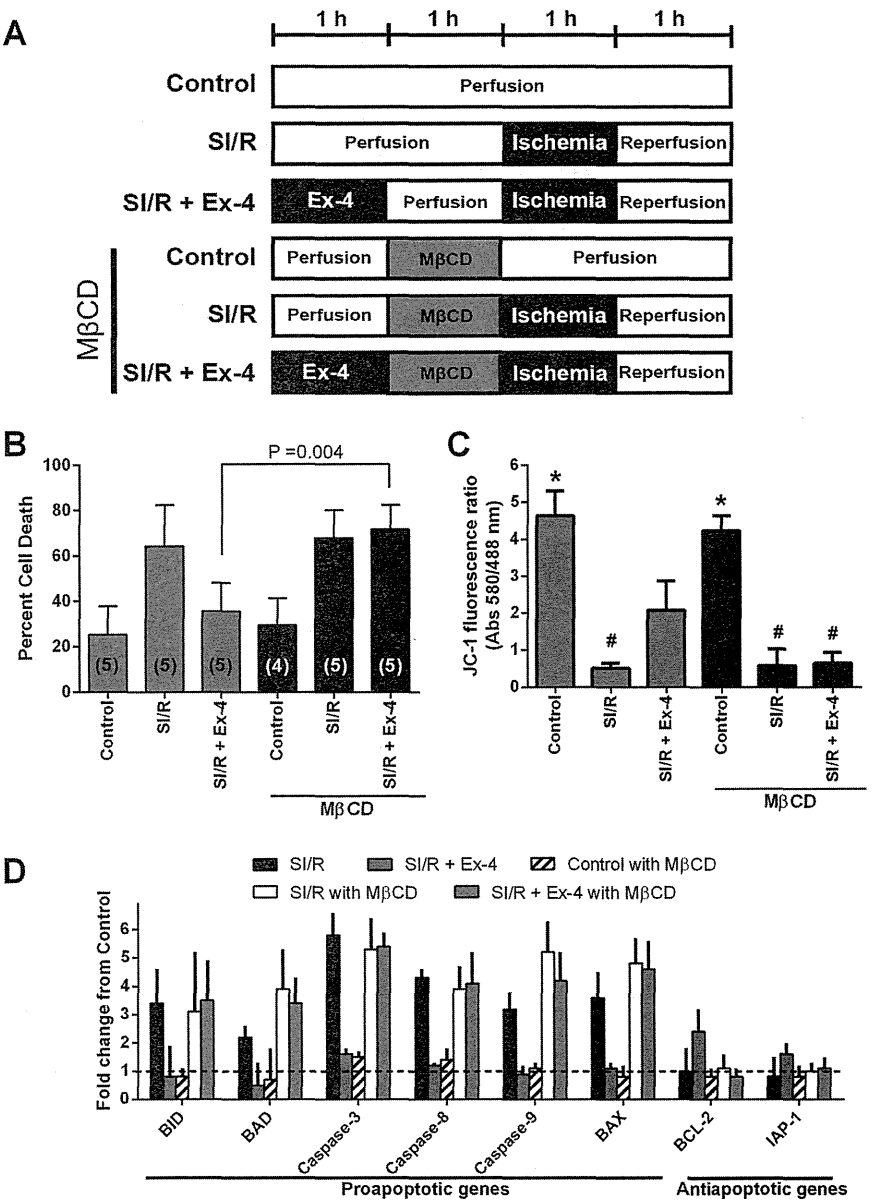

Figure 2 ***In vitro*** **assessment of the role of caveolae in exendin-4 (Ex-4) induced cardiac protection. (A)** Summary illustration of *in vitro* experimental groups. **(B)** Cardiac myocytes exposed to simulated ischemia/reperfusion (SI/R) were exposed to experimental procedures outlined in A. Cell death was determined by trypan blue staining. Cardiac myocytes under control conditions (Control) had minimal cell death. Methyl-β-cyclodextrin (MβCD) abolished the Ex-4 induced cardiac protection effect. Group sizes are indicated on the individual bars in parentheses. **(C)** Apoptotic changes were measured by investigating mitochondrial membrane potential using JC-1 after SI/R. The excitation rate (red/green) indicates changes within the mitochondrial membrane potential. *P < 0.001 vs. SI/R, SIR + Ex-4, SI/R with MβCD, and SI/R + Ex-4 with MβCD. #P < 0.05 vs. Control, SI/R + Ex-4, and Control with MβCD. n = 4 per each group. **(D)** Real-time polymerase chain reaction analysis of pro-apoptotic and anti-apoptotic gene expression after re-oxygenation. n = 4 per each group.

though there was a similar AAR in all groups of animals (Figure 5B). Cardiac troponin I (cTnI) levels were significantly attenuated by Ex-4 treatment in wild-type mice compared to control mice subjected to ischemia/reperfusion (36.9 ± 14.2 and 101.1 ± 22.3 ng/ml, P < 0.001); however, GLP-1 failed to reduce cTnI in Cav-3 KO mice and a level similar to control Cav-3 KO mice was observed (103.4 ± 38.4 and 96.8 ± 26.6 ng/ml, Figure 5C).

Discussion

In the current study, treatment with MβCD, an agent that has been shown to decrease the number of caveolae,

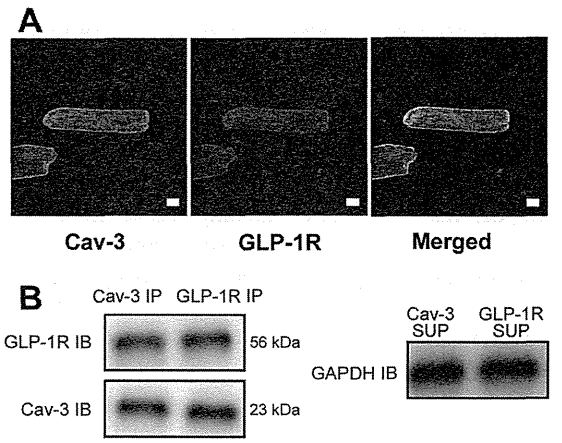

Figure 3 Glucagon-like peptide-1 receptor (GLP-1R) localization with caveolins or caveolae. (A) Immunofluorescence analysis of the expression and colocalization of caveolin-3 (Cav-3) and GLP-1R in cardiac myocytes. Fluorescent secondary antibodies were used to determine Cav-3 (green) and GLP-1R (red) localization, and strong colocalization (merged images, yellow) were observed on the cell surface membrane. Bar length = 10 μm. **(B)** The colocalization was confirmed by immunoprecipitation (IP). Immunoblot (IB) analysis detected Cav-3 and GLP-1R in Cav-3 and GLP-1R IP of cell lysates. Supernatants (SUP) from which the immunoprecipitates were generated were stained for GAPDH as loading controls.

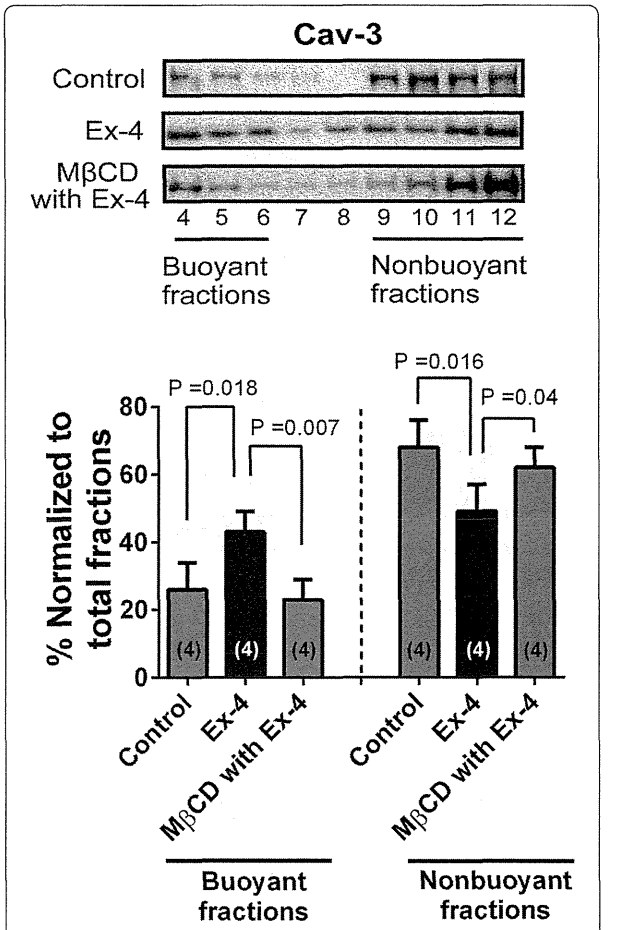

Figure 4 Lysed and fractionated hearts on sucrose density gradient. Fractions were collected and probed for caveolin-3 (Cav-3). We defined fractions 4–6 as buoyant membrane fractions enriched in caveolae and proteins associated with caveolae; fractions 9–12 were defined as nonbuoyant fractions, noncaveolar membranes. Fraction 7–8 were considered a transition zone and were not analyzed. Significant localization of Cav-3 in buoyant fractions was observed in the groups treated with exendin-4 (Ex-4), whereas control and methyl-β-cyclodextrin (MβCD)-treated with Ex-4 cells showed no effects on Cav-3 localization. Group sizes are indicated on the individual bars in parentheses.

produced an attenuation of Ex-4 (GLP-1R agonist) induced cardiac protection in *in vitro* models. Additionally, consistent with these findings, we observed that Ex-4 induced cardiac protection cannot be elicited in Cav-3 KO mice, indicating that the presence of caveolae (dependent on Cav-3 expression) is essential for myocardial protection in the *in vivo* mouse models. This is the first study to investigate the role of caveolins or caveolae in Ex-4 induced cardiac protection.

GLP-1 cardioprotection

Nutrient-responsive intestinal hormones including GLP-1 are rapidly metabolized by enzyme dipeptidyl-peptidase-4 (DPP-4) to generate an N-terminally truncated metabolite GLP-1 (9–36) [1,29]. Previous studies have demonstrated that the cardioprotective effect of exogenous GLP-1 were attributed to GLP-1R activation and subsequent recruitment of numerous intracellular signaling pathways involving protein kinase B, extracellular regulated kinases, p70S6K, and 5' adenosine monophosphate-activated protein kinase as well as downstream phosphorylation and inhibition of the pro-apoptotic protein BAD [5,6,30]. Hausenloy *et al.* also showed that chronic treatment with DPP-4 inhibitors reduce infarct size *via* the GLP-1R-protein kinase A pathway, in a glucose dependent manner *in vivo* rat models and confirmed the cardioprotective action of the endogenous intact GLP-1 on ischemia/reperfusion injury [31]. Moreover, Bao *et al.* [32] revealed that the long acting GLP-1R agonist could provide more sustained cardioprotective effect in the setting of acute myocardial ischemia/reperfusion injury than the short-acting Ex-4.

GLP-1 and the caveolin-dependent pathway

Caveolae, cholesterol and sphingolipid enriched invaginations of plasma membrane play a role physiological functions and vital to cardiac protective mechanisms. Caveolae and caveolins have been shown to play a fundamental role in the phenomenon of myocardial protection against ischemia/reperfusion injury [11-13]. In the present study, we investigated that wild-type mice

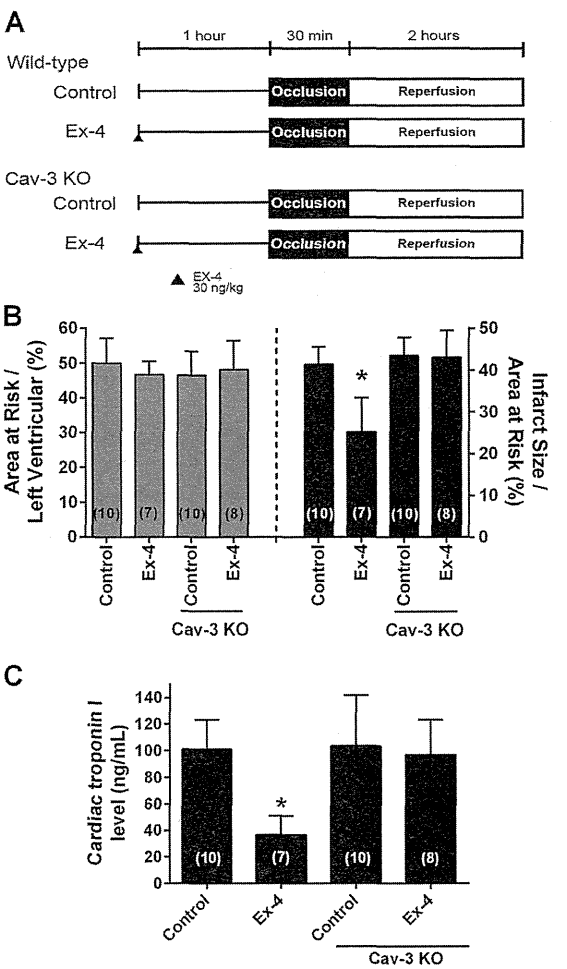

Figure 5 Caveolin-3 expression and reduction in infarct size. Mice underwent 30-min coronary artery occlusion followed by 2-h reperfusion after 24-h recovery from pretreatment with oxygen (Control) or exendin-4 (Ex-4) in wild-type and caveolin-3 knockout (Cav-3 KO) mice. **(A)** *In vivo* Ex-4 induced cardiac protection protocol. **(B)** Area at risk was calculated as a percentage of the left ventricle and revealed no significant differences between all groups. Ex-4 induced cardiac protection was abolished Cav-3 KO mice, as shown by no significant decrease in percent infarct size / area at risk when compared to control Cav-3 KO; however, a significant decrease in infarct size was observed between wild-type Ex-4 and Cav-3 KO Ex-4. **(C)** Cardiac troponin I, a marker of myocardial damage also revealed a significant decrease in Ex-4 treated control mice, but no effect in Cav-3 KO mice. Group sizes are indicated on the individual bars in parentheses. *P < 0.001 compared with Cav-3 KO pretreated with Ex-4.

treated with GLP-1 analogue, Ex-4, were protected against ischemia/reperfusion injury *in vivo*, whereas Cav-3 KO mice were not. In addition, Ex-4 protected isolated CM from hypoxia-induced cell death *in vitro* and had profound effects on membrane microdomains of CM. Our previous studies also revealed that Cav-3 KO mice, which decrease the number of myocardial caveolae, lose the ability to undergo cardioprotection from ischemia/reperfusion injury both *in vitro* and *in vivo* models [14-17]. Although there has been little evidence regarding the relationship between caveolae, caveolins and GLP-1R within the heart, other organ systems including human embryonic kidney (HEK) 293 cells and pancreatic β cells [33,34]. Syme *et al.* demonstrated that GLP-1 receptor interacts with Cav-1 in an association that is necessary for receptor trafficking to the cell membrane and signaling activity in HEK 293 cells [33]. Furthermore, Yang *et al.* demonstrated that activation peroxisome proliferator-activated receptor β/σ protects pancreatic β cells from apoptosis by upregulating the expression of GLP-1R, and sterol regulatory element binding protein-1c/Cav-1 pathway regulates GLP-1R expression [34].

In the present study, we showed that that GLP-1R interacted with Cav-3 and that the administration of Ex-4 led to cardiac protection. Caveolins can interact with a series of signaling molecules, including GPCRs *via* caveolin-binding motifs and may act as a molecular chaperone for GPCRs [12,13]. Overexpression of a dominant-negative form of Cav-1 or mutations within the Cav-1 binding domain of the GLP-1R attenuated GLP-1 binding and GLP-1R expression at the membrane [33]. Collectively, these data implicate that caveolae and caveolins are essential for GLP-1 induced cardiac protection by mediating the GLP-1R.

Hemodynamic effects of GLP-1

GLP-1 has been shown to increase blood pressure and heart rate in rats [35,36] although others failed to demonstrate any hemodynamic changes in the porcine models [37,38] and human studies [39-42]. In addition, Bose *et al.* investigated that the effects of GLP-1 infusion in rats subjected to 30 min ischemia and 120 min of reperfusion and observed that GLP-1 had no hemodynamic differences in their *in vivo* and *ex vivo* experimental models [5,30,43]. The hemodynamic effects of Ex-4 were also assessed in the animal models, in which dose-dependent increases in mean arterial pressure and heart rate were noted in rats [44]. In our *in vivo* studies, however, there were not any hemodynamic changes among the groups at the pre-occlusion time. This may be due to the dose and the timing of administration, Gardiner *et al.* showed that at a dose of 25 ng/kg i.v., Ex-4 had little effect, but at higher concentrations (250 ng/kg) significant tachycardia and pressor effects were noted for 60 min [44]. As the dose and time period used for cardiac protection in mice are not known, we selected the dosage and time of administration for Ex-4 based on the reports of Gardiner *et al.* to prevent any hemodynamic differences during pre-occlusion (250 ng/kg i.v. at 60 min before occlusion) [44]. Furthermore, GLP-1 has been shown to have central nervous effects on the control of blood pressure and heart rate [45]; however, this mechanism can be

Table 1 Hemodynamics

	Baseline	Pre-occlusion	Ischemia 30 min	Reperfusion 2 h
Heart rate, beats · min^{-1}				
WT Control	430 ± 26	426 ± 26	383 ± 39*#	363 ± 26*#
WT Ex-4	432 ± 16	413 ± 41	402 ± 16	398 ± 9
Cav-3 KO Control	413 ± 27	415 ± 25	383 ± 25	381 ± 32
Cav-3 KO Ex-4	416 ± 28	419 ± 26	376 ± 39	357 ± 36*#
Mean arterial pressure, mmHg				
WT Control	75 ± 6	75 ± 6	70 ± 6	65 ± 10*#
WT Ex-4	78 ± 5	75 ± 5	72 ± 7 70 ± 8	
Cav-3 KO Control	77 ± 4	75 ± 4	71 ± 3* 65 ± 6*#	
Cav-3 KO Ex-4	76 ± 5	75 ± 5	70 ± 3	66 ± 5*#
Rate-Pressure Product, beats · min^{-1} · mmHg · 10^3				
WT Control	32.0 ± 3.3	32.0 ± 1.4	26.7 ± 3.5*#	23.7 ± 4.7*#
WT Ex-4	33.6 ± 2.7	31.2 ± 4.1	29.2 ± 3.5	28.0 ± 3.6*
Cav-3 KO Control	31.9 ± 2.2	31.1 ± 2.6	27.0 ± 2.3*#	25.0 ± 3.5*#
Cav-3 KO Ex-4	31.5 ± 3.7	31.5 ± 3.2	26.4 ± 3.5*#	23.4 ± 2.6*#

Data are mean ± SD. Wild-type (WT) or caveolins-3 knockout (Cav-3 KO) mice were randomly exposed to exendin-4 (Ex-4).
*Significantly ($P < 0.05$) different from baseline (intragroup comparison).
#Significantly ($P < 0.05$) different from pre-occlusion (intragroup comparison).

avoided in the *in vitro* setting. In our *in vitro* mouse models, we used 3.0 nM Ex-4 concentration, consistent with previous study by Ban *et al.* in which 3.0 nM Ex-4 protect against after ischemia/reperfusion in isolated mouse hearts [4,10].

Study limitations

There are several limitations in the present study. First, we evaluated the GLP-1R dependent effects of Ex-4 in experiments that investigated ischemia/reperfusion injury. Recent studies suggest that GLP-1 (9–36), the metabolite that is generated by DPP-4 and 1000-fold lower affinity to GLP-1R [46], also improve LV contractile function and post-ischemic myocardial injury [47]. Furthermore, GLP-1R knockout mice have lower heart rate and blood pressure with an increase in cardiac mass and GLP-1 has been shown to protect perfused hearts from rodents lacking GLP-1R from ischemia [4]. These findings suggest that GLP-1 and its metabolite GLP-1 (9–36) may be capable of exerting GLP-1 receptor-independent pathways on the cardiovascular system [10]. Second, Cav-3 KO mice have a variety of deleterious phenotypes (*i.e.*, muscle degeneration, insulin resistance, and progressive cardiomyopathy with age) that may affect outcome after ischemia/reperfusion injury [19,48,49].

Clinical implications

As a regulator of glucose homeostasis, an exogenous GLP-1 analogue or potentiating endogenous GLP-1 by DPP-4 inhibitors show promise for the treatment of type 2 diabetes mellitus (T2DM) associated with cardiovascular disease. Moreover, there have been several clinical trials using GLP-1 as a therapy for cardiovascular disease in human subjects. Exenatide, an exogenous GLP-1 analogue, was found to be more beneficial than the other current regimens (DPP-4 inhibitors, insulin or tiazolidinediones), in reaching therapeutic goals recommended by the American Diabetes Association in the treatment of T2DM, which is also promising in the reduction of other co-morbidities such as cardiovascular risk [50]. Lonborg *et al.* [51] has shown that exenatide resulted in an increased salvage index among ST-segment elevation myocardial infarction patients with hyperglycemia and normoglycemia. Interestingly, endogenous circulating GLP-1 level was found to be increased in patients with high cardiovascular risk, suggesting it represents a contra-regulatory response in states of increased metabolic risk [52].

Conclusions

In conclusion, the current results demonstrate that GLP-1R co-localized with caveolae and caveolins-3 are essential for the cardiac protection induced by exendin-4 from ischemia/reperfusion injury.

Abbreviations

GLP-1R: Glucagon-like peptide-1 receptor; Cav-3: Caveolin-3; Cav-3 KO: Caveolins-3 knockout; MβCD: Methyl-β-cyclodextrin; SI/R: Simulated ischemia/reperfusion; CM: Cardiac myocytes; GLP-1: Glucagon-like peptide-1; GPCRs: G-protein-coupled receptor; Ex-4: Exendin-4; LV: Left ventricle; AAR: Area at risk; IS: Infarct size; cTnI: Cardiac troponin I; DPP-4: Dipeptidyl-peptidase-4; HEK: Human embryonic kidney; T2DM: Type 2 diabetes mellitus.

Competing interests
The authors declare that they have no competing interests.

Authors' contributions
Conceived and designed the experiments: YMT, RT. Performed the experiments: YMT, RT, EH, YS, AS. Analyzed the data: EH, KT. Drafting of the manuscript and critically revising the manuscript: YMT, EH. Extensive review and editing of manuscript: YI, UY, KT. All authors read and approved the final manuscript.

Acknowledgments
The project was supported by JSPS KAKENHI numbers 24592300, 25462405, and 60161486 from Japan Society for the Promotion of Science, Tokyo.

Author details
[1]Department of Anesthesiology, University of Tokushima, 3-18-15 Kuramoto, Tokushima, Japan. [2]Department of Nutrition, University of Tokushima, Tokushima, Japan. [3]Cardiovascular Research Institute, Yokohama City University, Yokohama, Japan.

Received: 4 July 2014 Accepted: 30 August 2014
Published: 7 September 2014

References

1. Drucker DJ: **The biology of incretin hormones.** *Cell Metab* 2006, **3**(3):153–165.
2. Davidson MH: **Cardiovascular effects of glucagonlike peptide-1 agonists.** *Am J Cardiol* 2011, **108**(3 Suppl):33B–41B.
3. Baggio LL, Drucker DJ: **Biology of incretins: GLP-1 and GIP.** *Gastroenterology* 2007, **132**(6):2131–2157.
4. Ban K, Noyan-Ashraf MH, Hoefer J, Bolz SS, Drucker DJ, Husain M: **Cardioprotective and vasodilatory actions of glucagon-like peptide 1 receptor are mediated through both glucagon-like peptide 1 receptor-dependent and -independent pathways.** *Circulation* 2008, **117**(18):2340–2350.
5. Bose AK, Mocanu MM, Carr RD, Brand CL, Yellon DM: **Glucagon-like peptide 1 can directly protect the heart against ischemia/reperfusion injury.** *Diabetes* 2005, **54**(1):146–151.
6. Noyan-Ashraf MH, Momen MA, Ban K, Sadi AM, Zhou YQ, Riazi AM, Baggio LL, Henkelman RM, Husain M, Drucker DJ: **GLP-1R agonist liraglutide activates cytoprotective pathways and improves outcomes after experimental myocardial infarction in mice.** *Diabetes* 2009, **58**(4):975–983.
7. Timmers L, Henriques JP, de Kleijn DP, Devries JH, Kemperman H, Steendijk P, Verlaan CW, Kerver M, Piek JJ, Doevendans PA, Pasterkamp G, Hoefer IE: **Exenatide reduces infarct size and improves cardiac function in a porcine model of ischemia and reperfusion injury.** *J Am Coll Cardiol* 2009, **53**(6):501–510.
8. Eng J, Kleinman WA, Singh L, Singh G, Raufman JP: **Isolation and characterization of exendin-4, an exendin-3 analogue, from Heloderma suspectum venom. Further evidence for an exendin receptor on dispersed acini from guinea pig pancreas.** *J Biol Chem* 1992, **267**(11):7402–7405.
9. Sonne DP, Engstrom T, Treiman M: **Protective effects of GLP-1 analogues exendin-4 and GLP-1(9–36) amide against ischemia-reperfusion injury in rat heart.** *Regul Pept* 2008, **146**(1–3):243–249.
10. Ban K, Kim KH, Cho CK, Sauve M, Diamandis EP, Backx PH, Drucker DJ, Husain M: **Glucagon-like peptide (GLP)-1(9–36) amide-mediated cytoprotection is blocked by exendin (9–39) yet does not require the known GLP-1 receptor.** *Endocrinology* 2010, **151**(4):1520–1531.
11. Stary CM, Tsutsumi YM, Patel PM, Head BP, Patel HH, Roth DM: **Caveolins: targeting pro-survival signaling in the heart and brain.** *Front Physiol* 2012, **3**:393.
12. Insel PA, Head BP, Ostrom RS, Patel HH, Swaney JS, Tang CM, Roth DM: **Caveolae and lipid rafts: G protein-coupled receptor signaling microdomains in cardiac myocytes.** *Ann N Y Acad Sci* 2005, **1047**:166–172.
13. Patel HH, Murray F, Insel PA: **G-protein-coupled receptor-signaling components in membrane raft and caveolae microdomains.** *Handb Exp Pharmacol* 2008, **186**:167–184.
14. Tsutsumi YM, Horikawa YT, Jennings MM, Kidd MW, Niesman IR, Yokoyama U, Head BP, Hagiwara Y, Ishikawa Y, Miyanohara A, Patel PM, Insel PA, Patel HH, Roth DM: **Cardiac-specific overexpression of caveolin-3 induces endogenous cardiac protection by mimicking ischemic preconditioning.** *Circulation* 2008, **118**(19):1979–1988.
15. Horikawa YT, Patel HH, Tsutsumi YM, Jennings MM, Kidd MW, Hagiwara Y, Ishikawa Y, Insel PA, Roth DM: **Caveolin-3 expression and caveolae are required for isoflurane-induced cardiac protection from hypoxia and ischemia/reperfusion injury.** *J Mol Cell Cardiol* 2008, **44**(1):123–130.
16. Tsutsumi YM, Kawaraguchi Y, Horikawa YT, Niesman IR, Kidd MW, Chin-Lee B, Head BP, Patel PM, Roth DM, Patel HH: **Role of caveolin-3 and glucose transporter-4 in isoflurane-induced delayed cardiac protection.** *Anesthesiology* 2010, **112**(5):1136–1145.
17. Tsutsumi YM, Kawaraguchi Y, Niesman IR, Patel HH, Roth DM: **Opioid-induced preconditioning is dependent on caveolin-3 expression.** *Anesth Analg* 2010, **111**(5):1117–1121.
18. Kilkenny C, Browne WJ, Cuthill IC, Emerson M, Altman DG: **Improving bioscience research reporting: the ARRIVE guidelines for reporting animal research.** *PLoS Biol* 2010, **8**(6):e1000412.
19. Hagiwara Y, Sasaoka T, Araishi K, Imamura M, Yorifuji H, Nonaka I, Ozawa E, Kikuchi T: **Caveolin-3 deficiency causes muscle degeneration in mice.** *Hum Mol Genet* 2000, **9**(20):3047–3054.
20. Tsutsumi Y, Oshita S, Kitahata H, Kuroda Y, Kawano T, Nakaya Y: **Blockade of adenosine triphosphate-sensitive potassium channels by thiamylal in rat ventricular myocytes.** *Anesthesiology* 2000, **92**(4):1154–1159.
21. Kawano T, Oshita S, Tsutsumi Y, Tomiyama Y, Kitahata H, Kuroda Y, Takahashi A, Nakaya Y: **Clinically relevant concentrations of propofol have no effect on adenosine triphosphate-sensitive potassium channels in rat ventricular myocytes.** *Anesthesiology* 2002, **96**(6):1472–1477.
22. Patel HH, Tsutsumi YM, Head BP, Niesman IR, Jennings M, Horikawa Y, Huang D, Moreno AL, Patel PM, Insel PA, Roth DM: **Mechanisms of cardiac protection from ischemia/reperfusion injury: a role for caveolae and caveolin-1.** *FASEB J* 2007, **21**(7):1565–1574.
23. Tsutsumi YM, Tsutsumi R, Horikawa YT, Sakai Y, Hamaguchi E, Ishikawa Y, Yokoyama U, Kasai A, Kambe N, Tanaka K: **Geranylgeranylacetone protects the heart via caveolae and caveolin-3.** *Life Sci* 2014, **101**(1–2):43–48.
24. Tsutsumi YM, Tsutsumi R, Mawatari K, Nakaya Y, Kinoshita M, Tanaka K, Oshita S: **Compound K, a metabolite of ginsenosides, induces cardiac protection mediated nitric oxide via Akt/PI3K pathway.** *Life Sci* 2011, **88**(15–16):725–729.
25. Tsutsumi YM, Patel HH, Lai NC, Takahashi T, Head BP, Roth DM: **Isoflurane produces sustained cardiac protection after ischemia-reperfusion injury in mice.** *Anesthesiology* 2006, **104**(3):495–502.
26. Hirose K, Tsutsumi YM, Tsutsumi R, Shono M, Katayama E, Kinoshita M, Tanaka K, Oshita S: **Role of the O-linked beta-N-acetylglucosamine in the cardioprotection induced by isoflurane.** *Anesthesiology* 2011, **115**(5):955–962.
27. Tsutsumi YM, Patel HH, Huang D, Roth DM: **Role of 12-lipoxygenase in volatile anesthetic-induced delayed preconditioning in mice.** *Am J Physiol Heart Circ Physiol* 2006, **291**(2):H979–H983.
28. Tsutsumi YM, Yokoyama T, Horikawa Y, Roth DM, Patel HH: **Reactive oxygen species trigger ischemic and pharmacological postconditioning: *In vivo* and *in vitro* characterization.** *Life Sci* 2007, **81**(15):1223–1227.
29. Green BD, Flatt PR, Bailey CJ: **Dipeptidyl peptidase IV (DPP IV) inhibitors: A newly emerging drug class for the treatment of type 2 diabetes.** *Diab Vasc Dis Res* 2006, **3**(3):159–165.
30. Bose AK, Mocanu MM, Carr RD, Yellon DM: **Myocardial ischaemia-reperfusion injury is attenuated by intact glucagon like peptide-1 (GLP-1) in the in vitro rat heart and may involve the p70s6K pathway.** *Cardiovasc Drugs Ther* 2007, **21**(4):253–256.
31. Hausenloy DJ, Whittington HJ, Wynne AM, Begum SS, Theodorou L, Riksen N, Mocanu MM, Yellon DM: **Dipeptidyl peptidase-4 inhibitors and GLP-1 reduce myocardial infarct size in a glucose-dependent manner.** *Cardiovasc Diabetol* 2013, **12**(1):154.
32. Bao W, Holt LJ, Prince RD, Jones GX, Aravindhan K, Szapacs M, Barbour AM, Jolivette LJ, Lepore JJ, Willette RN, DeAngelis E, Jucker BM: **Novel fusion of GLP-1 with a domain antibody to serum albumin prolongs protection against myocardial ischemia/reperfusion injury in the rat.** *Cardiovasc Diabetol* 2013, **12**:148.
33. Syme CA, Zhang L, Bisello A: **Caveolin-1 regulates cellular trafficking and function of the glucagon-like Peptide 1 receptor.** *Mol Endocrinol* 2006, **20**(12):3400–3411.
34. Yang Y, Tong Y, Gong M, Lu Y, Wang C, Zhou M, Yang Q, Mao T, Tong N: **Activation of PPARbeta/delta protects pancreatic beta cells from palmitate-induced apoptosis by upregulating the expression of GLP-1 receptor.** *Cell Signal* 2014, **26**(2):268–278.

35. Yamamoto H, Lee CE, Marcus JN, Williams TD, Overton JM, Lopez ME, Hollenberg AN, Baggio L, Saper CB, Drucker DJ, Elmquist JK: **Glucagon-like peptide-1 receptor stimulation increases blood pressure and heart rate and activates autonomic regulatory neurons.** *J Clin Invest* 2002, **110**(1):43–52.
36. Gardiner SM, March JE, Kemp PA, Bennett T, Baker DJ: **Possible involvement of GLP-1(9–36) in the regional haemodynamic effects of GLP-1(7–36) in conscious rats.** *Br J Pharmacol* 2010, **161**(1):92–102.
37. Deacon CF, Pridal L, Klarskov L, Olesen M, Holst JJ: **Glucagon-like peptide 1 undergoes differential tissue-specific metabolism in the anesthetized pig.** *Am J Physiol* 1996, **271**(3 Pt 1):E458–E464.
38. Kavianipour M, Ehlers MR, Malmberg K, Ronquist G, Ryden L, Wikstrom G, Gutniak M: **Glucagon-like peptide-1 (7–36) amide prevents the accumulation of pyruvate and lactate in the ischemic and non-ischemic porcine myocardium.** *Peptides* 2003, **24**(4):569–578.
39. Zander M, Madsbad S, Madsen JL, Holst JJ: **Effect of 6-week course of glucagon-like peptide 1 on glycaemic control, insulin sensitivity, and beta-cell function in type 2 diabetes: a parallel-group study.** *Lancet* 2002, **359**(9309):824–830.
40. Amori RE, Lau J, Pittas AG: **Efficacy and safety of incretin therapy in type 2 diabetes: systematic review and meta-analysis.** *JAMA* 2007, **298**(2):194–206.
41. Drucker DJ, Nauck MA: **The incretin system: glucagon-like peptide-1 receptor agonists and dipeptidyl peptidase-4 inhibitors in type 2 diabetes.** *Lancet* 2006, **368**(9548):1696–1705.
42. Inzucchi SE, McGuire DK: **New drugs for the treatment of diabetes: part II: Incretin-based therapy and beyond.** *Circulation* 2008, **117**(4):574–584.
43. Bose AK, Mocanu MM, Carr RD, Yellon DM: **Glucagon like peptide-1 is protective against myocardial ischemia/reperfusion injury when given either as a preconditioning mimetic or at reperfusion in an isolated rat heart model.** *Cardiovasc Drugs Ther* 2005, **19**(1):9–11.
44. Gardiner SM, March JE, Kemp PA, Bennett T: **Mesenteric vasoconstriction and hindquarters vasodilatation accompany the pressor actions of exendin-4 in conscious rats.** *J Pharmacol Exp Ther* 2006, **316**(2):852–859.
45. Barragan JM, Eng J, Rodriguez R, Blazquez E: **Neural contribution to the effect of glucagon-like peptide-1-(7–36) amide on arterial blood pressure in rats.** *Am J Physiol* 1999, **277**(5 Pt 1):E784–E791.
46. Deacon CF: **Circulation and degradation of GIP and GLP-1.** *Horm Metab Res* 2004, **36**(11–12):761–765.
47. Nikolaidis LA, Elahi D, Shen YT, Shannon RP: **Active metabolite of GLP-1 mediates myocardial glucose uptake and improves left ventricular performance in conscious dogs with dilated cardiomyopathy.** *Am J Physiol Heart Circ Physiol* 2005, **289**(6):H2401–H2408.
48. Woodman SE, Park DS, Cohen AW, Cheung MW, Chandra M, Shirani J, Tang B, Jelicks LA, Kitsis RN, Christ GJ, Factor SM, Tanowitz HB, Lisanti MP: **Caveolin-3 knock-out mice develop a progressive cardiomyopathy and show hyperactivation of the p42/44 MAPK cascade.** *J Biol Chem* 2002, **277**(41):38988–38997.
49. Oshikawa J, Otsu K, Toya Y, Tsunematsu T, Hankins R, Kawabe J, Minamisawa S, Umemura S, Hagiwara Y, Ishikawa Y: **Insulin resistance in skeletal muscles of caveolin-3-null mice.** *Proc Natl Acad Sci U S A* 2004, **101**(34):12670–12675.
50. Meloni AR, DeYoung MB, Han J, Best JH, Grimm M: **Treatment of patients with type 2 diabetes with exenatide once weekly versus oral glucose-lowering medications or insulin glargine: achievement of glycemic and cardiovascular goals.** *Cardiovasc Diabetol* 2013, **12**:48.
51. Lonborg J, Vejlstrup N, Kelbaek H, Nepper-Christensen L, Jorgensen E, Helqvist S, Holmvang L, Saunamaki K, Botker HE, Kim WY, Clemmensen P, Treiman M, Engstorm T: **Impact of acute hyperglycemia on myocardial infarct size, area at risk, and salvage in patients with STEMI and the association with exenatide treatment: results from a randomized study.** *Diabetes* 2014, **63**(7):2474–2485.
52. Piotrowski K, Becker M, Zugwurst J, Biller-Friedmann I, Spoettl G, Greif M, Leber AW, Becker A, Laubender RP, Lebherz C, Goeke B, Marx N, Parhofer KG, Lehrke M: **Circulating concentrations of GLP-1 are associated with coronary atherosclerosis in humans.** *Cardiovasc Diabetol* 2013, **12**:117.

doi:10.1186/s12933-014-0132-9
Cite this article as: Tsutsumi *et al.*: Exendin-4 ameliorates cardiac ischemia/reperfusion injury via caveolae and caveolins-3. *Cardiovascular Diabetology* 2014 13:132.

Radiotherapy and Oncology 111 (2014) 306–310

Contents lists available at ScienceDirect

Radiotherapy and Oncology

journal homepage: www.thegreenjournal.com

Intra-arterial radiochemotherapy

Retrograde superselective intra-arterial chemotherapy and daily concurrent radiotherapy for stage III and IV oral cancer: Analysis of therapeutic results in 112 cases

Kenji Mitsudo [a,*], Toshiyuki Koizumi [a], Masaki Iida [a], Toshinori Iwai [a], Hideyuki Nakashima [a], Senri Oguri [a], Mitomu Kioi [a], Makoto Hirota [a], Izumi Koike [b], Masaharu Hata [b], Iwai Tohnai [a]

[a] Department of Oral and Maxillofacial Surgery; and [b] Department of Radiology, Yokohama City University Graduate School of Medicine, Japan

ARTICLE INFO

Article history:
Received 7 April 2013
Received in revised form 19 January 2014
Accepted 9 March 2014
Available online 17 April 2014

Keywords:
Oral cancer
Chemoradiotherapy
Retrograde superselective intra-arterial infusion
Organ preservation
Survival rate

ABSTRACT

Purpose: To evaluate the therapeutic results and rate of organ preservation in patients with stage III or IV oral cancer treated with retrograde superselective intra-arterial chemotherapy and daily concurrent radiotherapy.

Materials and methods: One hundred and twelve patients with stage III and IV oral squamous cell carcinoma underwent intra-arterial chemoradiotherapy. Catheterization from the superficial temporal and occipital arteries was performed. Treatment consisted of superselective intra-arterial chemotherapy (docetaxel, total 60 mg/m^2, cisplatin, total 150 mg/m^2) and daily concurrent radiotherapy (total of 60 Gy) for 6 weeks.

Results: The median follow-up for all patients was 46.2 months (range, 10–76 months). After intra-arterial chemoradiotherapy, primary site complete response was achieved in 98 (87.5%) of 112 cases. Five-year survival and local control rates were 71.3% and 79.3%, respectively. Grade 3 or 4 toxicities included mucositis in 92.0%, neutropenia in 30.4%, dermatitis in 28.6%, anemia in 26.8%, and thrombocytopenia in 7.1% of patients. Grade 3 toxicities included dysphagia in 72.3%, nausea/vomiting in 21.4%, fever in 8.0%, and renal failure in 0.9% of patients.

Conclusion: Retrograde superselective intra-arterial chemotherapy and daily concurrent radiotherapy for stage III and IV oral cancer provided good overall survival and local control.

 Radiotherapy and Oncology 111 (2014) 306–310

For patients with locally advanced head and neck cancer, including the oral cavity, surgery with or without radiotherapy is widely accepted as the standard treatment and is thought to be the most effective curative therapy. However, extended surgery markedly causes loss of oral function, including swallowing and speech, and affects the patient's social life, reducing the quality of life (QOL). To preserve function while maintaining or improving locoregional control and survival rates, concurrent chemoradiotherapy (CRT) represents one of the standard treatment modalities for definitive treatment of locoregionally advanced squamous cell carcinoma of the head and neck, particularly in resectable advanced cases [1]. However, treatment results remain unsatisfactory. Superselective intra-arterial chemotherapy for head and neck cancer has the advantage of delivering a high concentration of the chemotherapeutic agents to the tumor bed. It can be classified into the following two types: selective arterial infusion through the femoral artery by Seldinger method [2]; and retrograde selective infusion via the superficial temporal artery (STA) and/or occipital artery (OA) [3–5]. Retrograde superselective intra-arterial chemotherapy with radiotherapy for advanced head and neck cancers has been developed over the last 20 years [3,4], and can be used to provide daily concurrent CRT for patients with advanced head and neck cancer. Treatment results from arterial injection therapy combined with radiotherapy for locally advanced oral cavity cancer have been reported to be similar to those of surgery, suggesting the usefulness of this treatment modality [6]. This method can be used for patients with T3, 4 head and neck cancer, and it may allow organ preservation, even in cases of locally advanced head and neck cancer [7]. The purpose of the present study was to evaluate therapeutic results and rate of organ preservation in 112 patients with stage III and IV (M0) oral cancer treated with retrograde superselective intra-arterial chemotherapy and daily concurrent radiotherapy.

* Corresponding author. Address: Department of Oral and Maxillofacial Surgery, Yokohama City University Graduate School of Medicine, 3-9 Fukuura, Kanazawa-ku, Yokohama, Kanagawa 236-0004, Japan.
E-mail address: mitsudo@yokohama-cu.ac.jp (K. Mitsudo).

http://dx.doi.org/10.1016/j.radonc.2014.03.005
0167-8140/

Materials and methods

Patients

Between August 2006 and July 2011, 118 patients with stage III and IV squamous cell carcinoma of the oral cavity and no evidence of distant metastasis when initially evaluated underwent retrograde superselective intra-arterial chemotherapy and daily concurrent radiotherapy. Six of these patients were found to be ineligible for the study: 2 due to a catheter infection, 1 due to pneumonia, 1 due to edema of neck and pharynx, 1 due to liver dysfunction, and 1 due to withdrawal of consent during treatment. Thus, 112 patients (78 male and 34 female; median age, 59 years; range, 28–87 years) were eligible for evaluation (Table 1). The primary lesion and cervical lymph nodes were assessed by positron emission tomography–computed tomography (PET–CT), magnetic resonance imaging (MRI) and ultrasound examination before treatment. Staging was performed according to the 2002 UICC staging system [8]. Patients who had received previous chemotherapy, radiotherapy, or surgery were excluded. Patients were required to have an Eastern Cooperative Oncology Group (ECOG) performance status (http://ecog.dfci.harvard.edu/general/perf_stat.html) of 0 or 1, a white blood cell count of at least 3500 cells/mm^3, a platelet count of at least 100,000/mm^3, and a hemoglobin level of at least 9 g/dL. Patients with cerebral infarction, or severe dysfunction of the liver, kidney, heart, or lung were ineligible. The primary tumor sites included the tongue ($n = 60$), upper gingiva ($n = 16$), lower gingiva ($n = 14$), floor of mouth ($n = 7$), buccal mucosa ($n = 6$), hard palate ($n = 4$), and other lesion ($n = 5$). Forty patients had stage III disease, and the remaining 72 had stage IV disease. The local institutional research board approved this study, and informed consent was obtained from each participant.

Retrograde superselective intra-arterial infusion procedure

Before treatment, 3-dimensional computed tomography angiography (3D-CTA) of the carotid artery was performed to identify the main tumor-feeding arteries and determine the morphology of the tumor-feeding artery originating from the external carotid artery. Catheterization from the STA was performed according to the method described by Tohnai et al. [3] and Fuwa et al. [4] (HFT method) [7]. A hook-shaped catheter (Medikit Corp., Tokyo, Japan) was superselectively inserted into the target artery and fixed to the periauricular skin. Catheterization from OA was performed according to the method of Iwai et al. [5]. When the tumor had 2 or more feeding arteries, catheters were inserted into the 2 arteries via STA and OA or bilaterally. After catheterization, flow check digital subtraction angiography (DSA) and angio-CT were performed in all cases. Angio-CT can help to detect tumors by confirming enhancement of the feeding area and enabling the catheter to be placed at the appropriate position. Furthermore, weekly confirmation of the feeding artery by injection of a small amount of indigo carmine is important. When catheterization using a hook-shaped catheter was not stable, the guidewire exchange method was used to replace it with a P–U catheter (Toray Medical Co., Ltd., Tokyo, Japan) [4].

Table 1
Patients and disease characteristic ($n = 112$).

Characteristics	No. of patients (%)
Gender	
Male	78 (70)
Female	34 (30)
Age, year	
Range	28–87
Median	59
Primary tumor site	
Tongue	60 (54)
Upper gingiva	16 (14)
Lower gingiva	14 (13)
Floor of mouth	7 (6)
Buccal mucosa	6 (5)
Hard palate	4 (4)
Other	5 (4)
T classification	
T2	18 (16)
T3	43 (38)
T4a	47 (42)
T4b	4 (4)
Stage classification	
III	40 (36)
IVA	61 (54)
IVB	11 (10)
Total	112 (100)

UICC staging system, Sobbin et al.

Radiotherapy

Radiotherapy was planned for all patients after appropriate immobilization using a thermoplastic mask and 3-dimensional CT-based techniques. Conventional radiotherapy was performed at 4 or 6 MV and 2 Gy/fraction/day. The irradiation field was changed according to lymph node status. In cases of N0 disease, the field contained the primary site and levels I to III of the neck on the ipsilateral side. The dose was delivered to 40 Gy/20 fractions. The portal was then reduced to only the primary site to spare the spinal cord. The total dose delivered to the primary tumor was 60 Gy/30 fractions. In cases of N1–N2a, b disease, the field contained the primary site and the levels I–V of the neck on the ipsilateral side. The dose was delivered to 40 Gy/20 fractions. The portal was then reduced to the primary site and lymph node metastases. The total dose delivered to the primary tumor was 60 Gy/30 fractions, and that to the metastatic lymph node sites was 50 Gy/25 fractions. In cases of N2c disease, the field contained the primary site and the levels I–V of the neck on bilateral sides. The dose was delivered to 40 Gy/20 fractions. The portal was then reduced to the primary site and lymph node metastases. The dose to the spinal cord ranged from 40 to 45 Gy. The total dose delivered to the primary tumor was 60 Gy/30 fractions, and, if at all possible, the total dose delivered to the metastatic lymph node sites was to 50 Gy/25 fractions.

Superselective intra-arterial chemotherapy

The anticancer agent was injected in a bolus for 1 h through the intra-arterial catheter when radiotherapy was performed. The total dose of docetaxel (DOC) was 60 mg/m^2 (10 mg/m^2/week), and that of cisplatin (CDDP) was 150 mg/m^2 (5 mg/m^2/day) (Fig 1). Sodium thiosulfate (STS) (1 g/m^2) was administered intravenously to provide effective cisplatin neutralization after the anticancer agent was given as soon as possible. All patients were given a 5-HT3 receptor antagonist before administration of the anticancer agent.

Follow-up after the treatment

All patients were evaluated 4 weeks after completion of treatment by PET–CT, MRI and ultrasound examination. The purpose of this combined CRT using retrograde superselective intra-arterial infusion was to improve the local control rate and achieve good QOL without surgery. If residual primary tumor was present after this treatment, a salvage operation was performed 6–8 weeks after completion of intra-arterial CRT. If residual metastatic lymph nodes were present after treatment, radical neck dissection was performed.

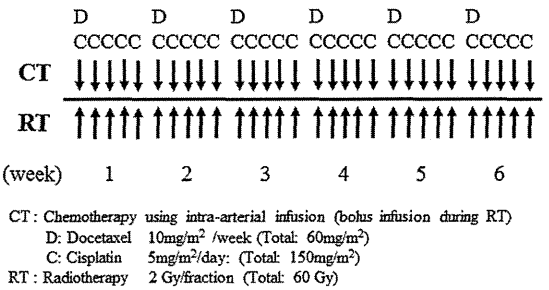

Fig. 1. Treatment schedule for chemoradiotherapy using retrograde superselective intra-arterial infusion. The total dose of docetaxel (DOC) was 60 mg/m^2 (10 mg/m^2/week × 6), and that of cisplatin (CDDP) was 150 mg/m^2 (5 mg/m^2/day × 30). When catheters were inserted into the 2 arteries or bilaterally, a half dose of anticancer agents was injected into the two lines, respectively. External irradiation was performed 5 times a week at 2 Gy per fraction, to a total of 60 Gy, for 6 weeks.

Toxicity assessment

Toxicities encountered during therapy were evaluated according to the National Cancer Institute – Common Terminology Criteria for Adverse Events v3.0 (http://ctep.cancer.gov/protocolDevelopment/electronic_applications/docs/ctcaev3.pdf). The evaluation categories were blood cell counts, nausea/vomiting, oral mucositis, dermatitis, dysphagia, renal function and fever.

Statistical analysis

Overall survival (OS) and local control (LC) rates were estimated using the Kaplan–Meier method. Cases of residual or recurrent primary lesion after treatment were considered to be local failures unless salvage operation was successful. The differences between stage III and stage IV OS and LC rates were assessed by the log-rank test.

Results

Treatment results

For all patients, the median follow-up was 46.2 months (range, 10–76 months). After intra-arterial chemoradiotherapy, primary site complete response was achieved in 98 (87.5%) of 112 cases, and residual tumor was seen in 14 (12.5%) cases. Eight patients (7.1%) was detected local recurrence during follow-up. Thirty patients (26.8%) died: 21 of pulmonary metastasis, 5 of progression of the primary lesion, 3 of the cervical lymph node, and 1 of non-cancer-related causes.

The Kaplan–Meier method was used to estimate the 1-year, 3-year, and 5-year OS rates, which were 85.7%, 74.6%, and 71.3%, respectively (Fig. 2a). At 5 years, OS rates of stage III and stage IV oral cancer patients were 83.1% and 64.5%, respectively. Five-year OS rate of stage III oral cancer patients was significantly higher than that of stage IV oral cancer patients ($P = 0.033$) (Fig. 2a). The 1-year, 3-year, and 5-year LC rates were 82.0%, 79.3%, and 79.3%, respectively (Fig. 2b). At 5 years, LC rates of stage III and stage IV oral cancer patients were 85.1% and 75.4%, respectively. No significant difference was observed between the LC rates of stage III and stage IV oral cancer patients ($P = 0.120$) (Fig. 2b).

Toxicities

Table 2 shows the acute toxicities experienced during therapy. Grade 3 or 4 toxicities included mucositis in 103 cases (92.0%), neutropenia in 34 cases (30.4%), dermatitis in 32 cases (28.6%), anemia in 30 cases (26.8%), and thrombocytopenia in 8 case (7.1%). Grade 3 dysphagia occurred in 81 cases (72.3%) with severe mucositis. Grade 3 toxicities included nausea/vomiting in 24 cases

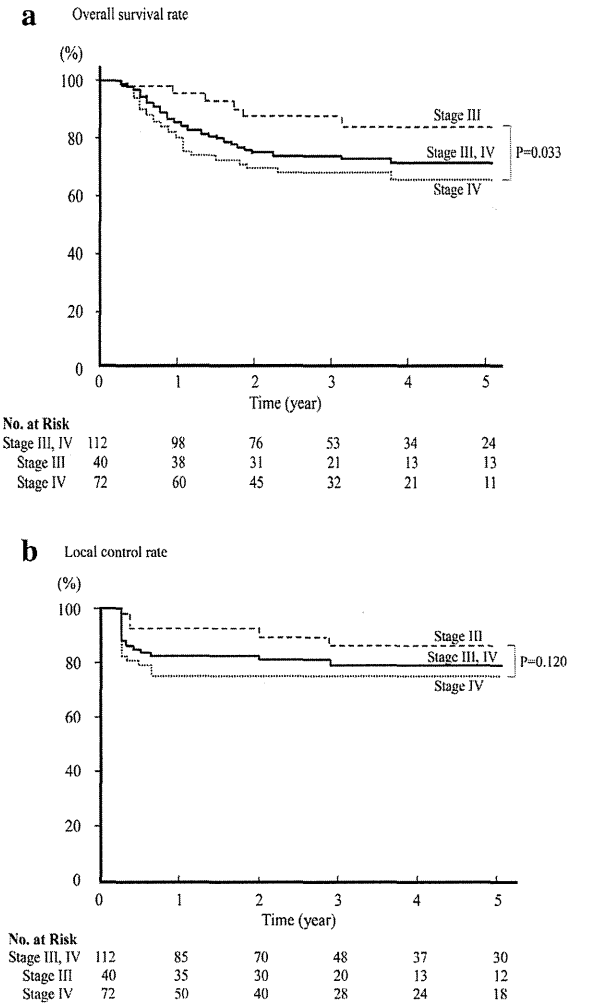

Fig. 2. Overall survival rate (a) and local control rate (b) using the Kaplan–Meier method. (a) Three and 5-year OS rates were 74.6%, and 71.3%, respectively. At 5 years, the OS rate of stage III oral cancer patients was 83.1% (95% confidence interval, 80.8–85.3%), and the OS rate of stage IV oral cancer patients was 64.5% (95% confidence interval, 61.0–67.9%), 5-year OS rate of stage III oral cancer patients was significantly higher than that of stage IV oral cancer patients ($P = 0.033$). (b) Three and 5-year LC rates were 79.3% and 79.3%, respectively. At 5 years, the LC rate of stage III oral cancer patients was 85.1% (95% confidence interval, 83.3–86.1%), and, the LC rate of stage IV oral cancer patients was 76.1% (95% confidence interval, 73.6–77.3%); no significant difference was observed between the LC rates of stage III and stage IV oral cancer patients ($P = 0.120$).

Table 2
Toxicity ($n = 112$).

Toxicity	No. of patients by toxicity grade			
	I	II	III	IV
Neutropenia	15	22	31	3
Anemia	36	39	26	4
Thrombocytopenia	56	5	6	2
Nausea/Vomiting	23	31	24	
Mucositis		9	54	49
Dermatitis	13	61	28	4
Dysphagia	1	22	81	
Renal failure	27	3	1	
Fever	37	24	9	

National Cancer Institute – Common Terminology Criteria for Adverse Events v3.0.